

Anti-microtubule activity of the traditional Chinese medicine herb Northern Ban Lan (*Isatis tinctoria*) leads to glucobrassicin^{oo}

Pingyin Guan¹, Jianning Zhou¹, Sergey Girel², Xin Zhu¹, Marian Schwab¹, Kunxi Zhang¹, Qiyan Wang-Müller³, Laurent Bigler² and Peter Nick^{1*}

1. Molecular Cell Biology, Botanical Institute, Karlsruhe Institute of Technology, Fritz-Haber-Weg 4, Karlsruhe 76131, Germany

2. Department of Chemistry, University of Zürich, Winterthurerstr.190, CH-8057, Zürich, Switzerland

3. Research Institute of Organic Agriculture FiBL, Ackerstrasse 113, CH-5070, Frick, Switzerland

Present address: Pingyin Guan, College of Horticulture, China Agricultural University, Beijing 100193, China

Present address: Sergey Girel, Institute of Pharmaceutical Sciences of Western Switzerland, University of Geneva, Rue Michel-Servet 1, CH-1211, Geneva 4, Switzerland

Present address: Qiyan Wang-Müller, Swiss Chinese Herbal Medicine and Functional Food Innovation Center, Mainaustrasse 21, CH-8046, Zürich, Switzerland

*Correspondence: Peter Nick (peter.nick@kit.edu)



Pingyin Guan



Peter Nick

activity-guided fractionation to screen out the biologically active compounds of *I. tinctoria*. Among 54 fractions obtained from either leaves or roots of *I. tinctoria* by methanol (MeOH/H₂O 8:2), or ethyl acetate extraction, one specific methanolic root fraction was selected, because it efficiently and rapidly eliminated microtubules. By combination of further purification with ultra-high-performance liquid chromatography and high-resolution tandem mass spectrometry most of the bioactivity could be assigned to the glucosinolate compound glucobrassicin. Glucobrassicin can also affect microtubules and induce apoptosis in HeLa cells. In the light of these findings, the antiviral activity of Northern Ban Lan is discussed in the context of microtubules being hijacked by many viral pathogens for cell-to-cell spread.

Keywords: anti-microtubule activity, cytoskeleton, glucobrassicin, high-performance liquid chromatography (HPLC), high-resolution tandem mass spectrometry (HRMS/MS), *Isatis tinctoria*, Northern Ban Lan, traditional Chinese medicine (TCM)

Guan, P., Zhou, J., Girel, S., Zhu, X., Schwab, M., Zhang, K., Wang-Müller, Q., Bigler, L., and Nick, P. (2021). Anti-microtubule activity of the traditional Chinese medicine herb Northern Ban Lan (*Isatis tinctoria*) leads to glucobrassicin. *J. Integr. Plant Biol.* **63**: 2058–2074.

ABSTRACT

Traditional Chinese medicine (TCM) belongs to the most elaborate and extensive systems of plant-based healing. The herb Northern Ban Lan (*Isatis tinctoria*) is famous for its antiviral and anti-inflammatory activity. Although numerous components isolated from *I. tinctoria* have been characterized so far, their modes of action have remained unclear. Here, we show that extracts from *I. tinctoria* exert anti-microtubular activity. Using time-lapse microscopy in living tobacco BY-2 (*Nicotiana tabacum* L. cv Bright Yellow 2) cells expressing green fluorescent protein-tubulin, we use

INTRODUCTION

Medicinal plants have been of great importance in the management of human diseases. The finding that even our closest living relatives, the chimpanzees, have developed a culture to use specific plants for healing purposes (Page et al., 1992), indicates that, from prehistoric time, humankind have used plants for healing. Classical examples are the Neem tree (*Azadirachta indica*) (reviewed in Kumar and Navaratnam, 2013), and the bark of the willow tree (*Salicis cortex*) (for reviews see Jack, 1997; Mahdi, 2010). To date, half a million of plant secondary metabolites with known biological activities are considered as a sustainable source of novel drug candidates for the pharmacological treatment of various diseases (recent reviews in Demain and Vaishnav, 2011; David et al., 2015; Shen, 2015; Bernardini et al., 2018). Numerous effective drugs with economic impact are of herbal origin, such as the alkaloids morphine (*Papaverum somniferum* L.), paclitaxel (*Taxus brevifolia*), digitoxin (*Digitalis purpurea*), curare (*Chondrodendron tomentosum*), or the sesquiterpene artemisinin (qinghaosu 青蒿素 in Chinese, *Artemisia annua*), are still isolated from herbal plants (for reviews see Mahdi, 2010; Shen, 2015; Bernardini et al., 2018). Others, such as aspirin (acetyl-salicylic acid), while being meanwhile synthesized technically, derive from plants as well (*Salix* sp.). Thus, the impact of pharmacology of natural products from medicinal plants for the discovery of novel drugs is considerable, reviving the interest in traditional systems of healing, but also fueling controversies about the intellectual property linked with this traditional knowledge (Fredriksson, 2017).

Traditional Chinese medicine (TCM) belongs to the most elaborate systems of healing (Waller, 1998). The compendium *Bencao Gangmu* by Shizhen Li, published in 1578, lists more than 10,000 recipes, based on 1,892 plant species, forms the base of the current TCM pharmacopeia (Xu et al., 2019). This extensive body of traditional knowledge represents a huge, still almost untapped, reservoir for the discovery of new bioactive compounds. In the context of the current Covid-19 pandemic, TCM plants with antiviral activity have attracted attention. Northern Ban Lan is traditionally used for its antiviral activity, but also to cure a broad spectrum of other diseases (for review see Hamburger, 2002) due to its anti-inflammatory and anti-microbial effect (Recio et al., 2006a, 2006b; Brattström et al., 2010; Ullah et al., 2017). While true Northern Ban Lan is supposed to be *Isatis tinctoria* (Dyer's woad), often the more easily accessible, closely related *I. indigotica* (indigo) is used as a substitute. Both the root (*I. radix*, Ban Lan Gen, 板蓝根 in Chinese), and the leaf (*I. folia*, Da Qing Ye, 大青叶 in Chinese) are used for the clinical treatment of virus-related respiratory diseases such as severe acute respiratory syndrome (SARS), and H1N1 (Lin et al., 2005; Wang et al., 2011). Currently, Northern Ban Lan is subject to several clinical trials for therapies against Covid-19 (for a recent review see Yang et al., 2020).

The medical activities of *Isatis* extract are thought to depend on the synergistic effect of multiple components (Zhou and Zhang, 2013). Over the last decades, more than 100

bioactive constituents have been identified in methanolic extracts of *I. tinctoria* leaves and roots, including numerous alkaloids, fatty acids, and carotenoids (Mohn et al., 2009), as well as phenylpropanoid derivatives, such as flavonoids, hydroxyl-cinnamic and hydroxyl-benzoic acid derivatives, or mono- and oligo-lignols (Nguyen et al., 2017). Especially, the glucosinolates, indole-derived compounds, have attracted interest for their prospective medical properties (Mohn and Hamburger, 2008; Nguyen et al., 2017). For instance, indirubin, a bis-indole alkaloid, was reported to mitigate expression of the influenza infection marker RANTES (regulated on activation, normal T cell expressed and secreted) in a bronchitis cell model (Mak et al., 2004; Sethi et al., 2006). Although these phenomena appear as quite distant, they are functionally linked, namely by microtubules: influenza viruses hijack the microtubules of their hosts for intracellular movement, uncoating, and exit from the cell (for a recent review see Simpson and Yamauchi, 2020). Also the transcription factor nuclear factor- κ B is tethered to microtubules and can, upon modulation of microtubule dynamics, activate apoptosis (Rai et al., 2015).

Microtubules are dynamic components of the cytoskeleton in eukaryotic cells, which are essential for various cellular functions, such as development and maintenance of cell shape, intracellular transport of vesicles and other components, cell signaling and cell division (see reviews in Dumontet and Jordan, 2010; Forth and Kapoor, 2017; Lu and Gelfand, 2017; Muroyama and Lechler, 2017; Dogterom and Koenderink, 2019). Interference with microtubular dynamics by small-molecule inhibitors leads to mitotic arrest and can trigger apoptosis (reviewed in Peterson and Mitchison, 2002; Florian and Mitchison, 2016). For this reason, anti-microtubular compounds are among the most effective drugs used in the treatment of solid tumors and hematological malignancies (for reviews see Jordan et al., 1998; Kaul et al., 2019). Over the past decades, a large number of microtubule-targeting compounds have been discovered during large-scale screens of natural products, and obtained approval for cancer therapy (reviewed in Altmann and Gertsch, 2007; Florian and Mitchison, 2016; Mahaddalkar and Lopus, 2017). Furthermore, microtubules are used for the transport of RNA, which is a central element of morphogenesis. A classic example is the microtubule-dependent transport of maternal messenger RNA (mRNA) during polarization of the *Drosophila* embryo (St Johnston and Nüsslein-Volhard, 1992), or the long-distance transport of mRNA in neurons (reviewed in Glock et al., 2017). Several RNA viruses hijack this essential function for their own purpose, for instance to move from the plasma membrane to the nuclear envelope (Wang et al., 2017). Anti-microtubule agents might, therefore, affect virus infection. The fact that also plant microtubules are usurped for transport of RNA viruses (tobacco mosaic virus: Heinlein et al., 1995; grapevine fan leaf virus: Laporte et al., 2003), indicates that, here, an evolutionary ancient target is exploited, which is shared between plants and animals.

However, not only viruses, but also plants themselves, use microtubules as targets for chemical warfare. For instance, the monoterpene citral is used to suppress germination of

competing plants by blocking the division spindle (Chaimovitch et al., 2010), and several alkaloids serve to ward off herbivores, by affecting integrity or dynamics of their microtubules. Among those, *Vinca* alkaloids and taxanes are of medical relevance, because they are widely used for tumor therapy (Nogales et al., 1995; Jordan et al., 1998). While being relatively conserved, tubulins of plants and animals also have evolved minor, but specific differences that lead to specificity of such plant-derived anti-microtubule compounds (for review see Dostál and Libusová, 2014). Nevertheless, in contrast to the microtubule-associated proteins, the molecular conservation of tubulins is very high – for instance, porcine brain tubulin can be micro-injected into living plant cells and integrates readily with the host cytoskeleton and then participates normally even in very specific responses (Himmelspach et al., 1999).

Based on the conservation of tubulins between animals and plants, we ventured to search for anti-microtubule compounds from *I. tinctoria* (Northern Ban Lan) using activity-guided high-performance liquid chromatography (HPLC) fractionation as strategy. We deliberately chose a plant-cell system as readout for bioactivity. The use of a tobacco cell line, where microtubules are labeled by green fluorescent protein (GFP)-tagged plant tubulin (Kumagai et al., 2001), not only allowed us to follow the response of microtubules *in vivo*, but also selected for activities that are directed to targets shared between mammalian and plant cells: While the microtubule-associated proteins are quite divergent between these two cell types, a bioactivity seen on plant microtubules is most likely acting on the level of the evolutionarily conserved tubulins themselves. Using high-resolution mass spectrometry (HRMS) and tandem mass spectrometry (MS/MS), our search identified glucobrassicin as an anti-microtubule compound from the TCM plant Northern Ban Lan (*I. tinctoria*).

RESULTS

Anti-microtubular activity of *I. tinctoria* roots originates from a specific fraction

Leaf and root material from *I. tinctoria* was extracted with two different solvent systems, either MeOH/H₂O 8:2, or ethyl acetate (EtOAc) (yields are shown in Table S1, representative liquid chromatography ultra violet chromatograms in Figure S1). These crude extracts were fractionated at fixed retention time (t_R) intervals, and the resulting fractions were screened for their ability to induce a response of GFP-tagged microtubules in tobacco Bright Yellow 2 (BY-2) cells expressing GFP-NtTuA3 (*Nicotiana tabacum* α -tubulin-3) as readout for bioactivity. According to the differentiation of extraction material (leaf, root) and solvent (MeOH, EtOAc), the total 54 fractions were named ML-1 to ML-14 (MeOH/H₂O 8:2 leaf fractions), EL-1 to EL-12 (EtOAc leaf fractions), MR-1 to MR-14 (MeOH/H₂O 8:2 root fractions), and ER-1 to ER-14 (EtOAc root fractions), respectively (Table S3).

These fractions were then administered to expanding cells of microtubular marker line TuA3-GFP to probe for potential

effects upon cortical microtubules. In the solvent control, microtubules were arranged in parallel bundles aligned perpendicular to the expansion axis of the cell, as it is typical for elongating cells (Figure S2). In fact, some fractions induced perturbations in the integrity and the organization of cortical microtubules, while others did not produce any effect. For instance, out of the 14 fractions obtained by methanolic extraction of leaves, only three (ML-4, ML-5, and ML-10) were able to induce microtubular perturbations (Figure S2, white arrows). This effect was relatively swift, as shown by a time course experiment (Figure S3). For the more active fractions ML-5 and ML-10, a clear disassembly of cortical microtubules was visible already from 15 min after application. Considering the EtOAc leaf extracts, two fractions (EL-3, EL-9) produced the microtubule elimination (Figure S4). Also these fractions affected microtubules strongly from 15 min after application (Figure S5). Methanolic extraction of the roots yielded one fraction (MR-1), which was more active with respect to microtubule elimination than any other fraction recovered in this study (Figure S6). As early as 10 min, most of the microtubules had disappeared (Figure S7). However, extraction of roots with EtOAc yielded only one fraction (ER-9) with a very mild effect (Figure S8). This mild effect became evident from around 20 min (Figure S9). The microtubule activities of the different fractions are summarized in Table S5: In total, three MeOH/H₂O 8:2 (ML-4, ML-5, and ML-10), two EtOAc fractions (EL-3, EL-9) from leaves were screened out. For roots only one MeOH/H₂O 8:2 (MR-1) and one EtOAc fraction (ER-9) displayed anti-microtubular activity. Among these seven active fractions, MR-1 induced the strongest microtubule response and was therefore put into the focus of subsequent analysis.

The most active fraction MR-1 was as efficient as the anti-microtubular herbicide Oryzalin (Figure 1A). A quantification of microtubule integrity revealed that none of the other root fractions caused any significant response of microtubules (Figure 1B). This response was also seen for dilutions of MR-1 (Figure 2). For instance, a dilution of 1:5 made microtubules disappear from as early as 3 min. As early as 10 min, most microtubules had been eliminated, and only punctate remnants of microtubules were seen, probably corresponding to microtubule organizing centers (MTOCs). For the 1–10 dilution, there was no observable change over the first 15 min, but from 20 min some fluorescent dots appeared, indicative of a slight effect upon microtubules.

The effect of fraction MR-1 is specific for microtubules

The efficient elimination of microtubules by the most active fraction MR-1 might be an unspecific consequence of a potential cytotoxicity. We checked, therefore, whether MR-1 would also disrupt actin filaments, as a second element of the plant cytoskeleton, and whether this fraction exerts phytotoxic effects. For this purpose, we employed the actin marker line GF11 (Sano et al., 2005), where actin filaments are tagged by the actin-binding domain 2 of plant fimbrin in fusion with GFP. Even after treatment with MR-1 for 60 min in the same dilutions

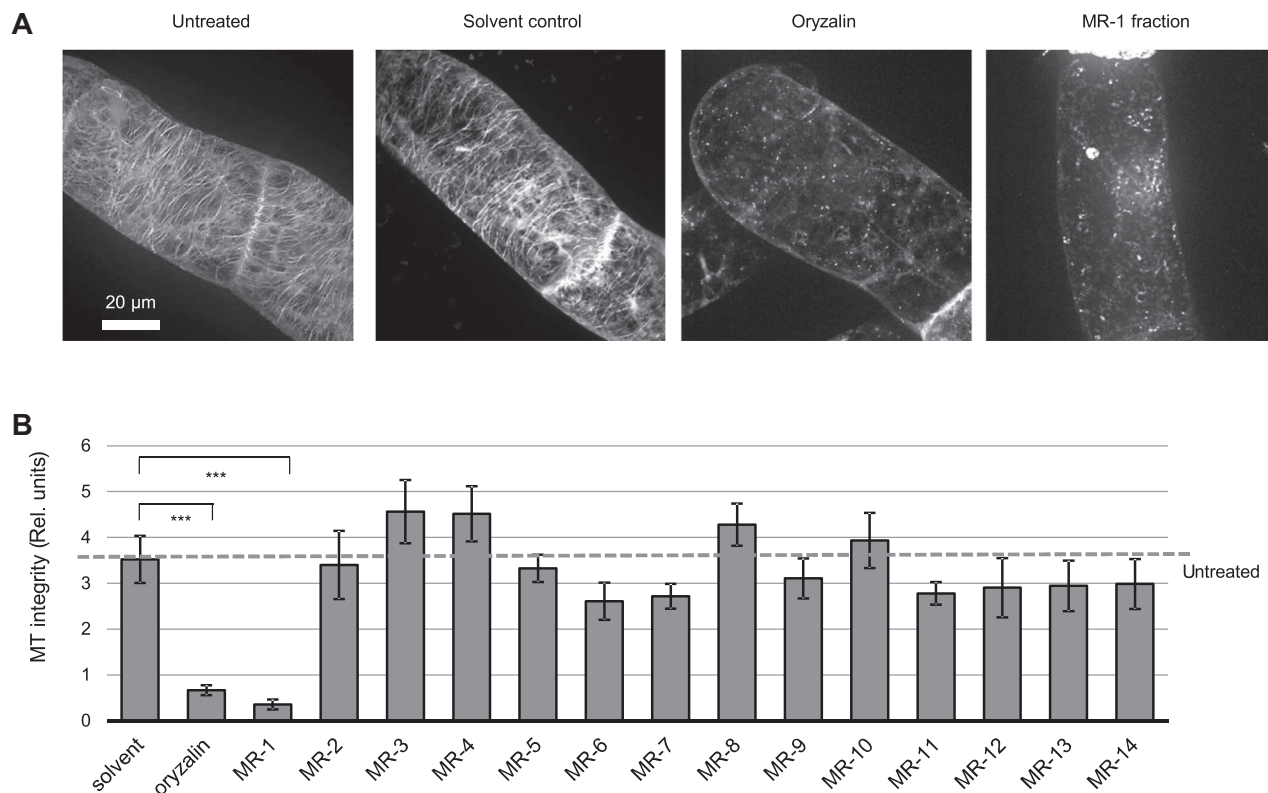


Figure 1. Response of microtubules to treatment with fractions obtained from MeOH/H₂O 8:2 extracts of *Isatis tinctoria* roots in the microtubule marker line *Nicotiana tabacum* L. cv Bright Yellow 2 α -tubulin-3 green fluorescent protein (BY-2 TuA3-GFP)
(A) Representative cells after 60 min of treatment with the solvent control (1% dimethyl sulfoxide), the anti-microtubular herbicide Oryzalin as positive control, and fraction MR-1 as compared to untreated cells observed by spinning-disc microscopy. Geometrical projections from z-stacks collected at intervals of 0.5 μ m are shown. **(B)** Quantification of microtubule integrity for the 14 methanolic fractions obtained from *I. tinctoria* root (MR-1 to MR-14), as compared to untreated cells, control, solvent control, and the positive control Oryzalin. ***Difference significant at $P < 0.001$ based on a *t*-test.

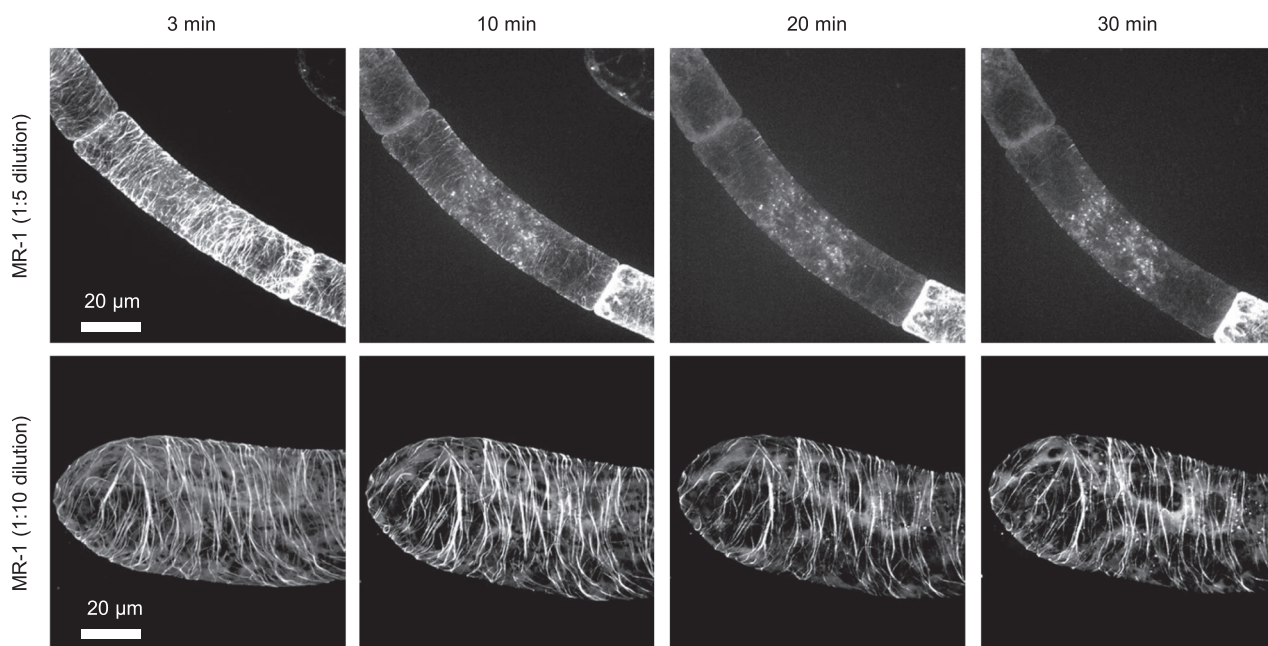


Figure 2. Time-lapse study of the microtubular response to a 1:5 dilution (upper row) and a 1:10 dilution (lower row) of the methanolic root fraction MR-1 in expanding cells of the microtubule marker line *Nicotiana tabacum* L. cv Bright Yellow 2 α -tubulin-3 green fluorescent protein (BY-2 TuA3-GFP) followed over 30 min
 Geometrical projections from z-stacks collected at intervals of 0.5 μ m are shown.

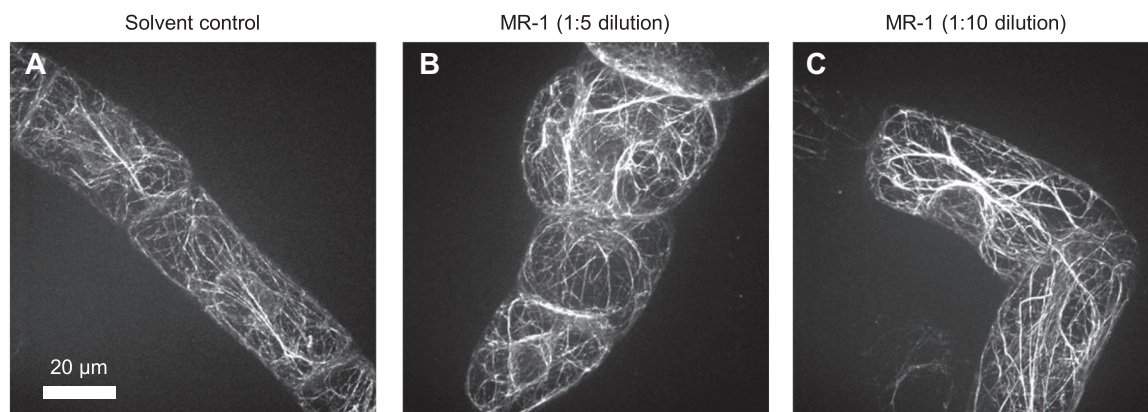


Figure 3. Response of actin filaments to the methanolic root fraction MR-1 in expanding cells of the actin marker line *Nicotiana tabacum* L. cv Bright Yellow 2 α -tubulin-3 green fluorescent protein (BY-2 TuA3-GFP) 30 min after application

(A) Solvent control, (B) 1:5 dilution, (C) 1:10 dilution. Geometrical projections from z-stacks collected at intervals of 0.5 μ m are shown for representative cells.

as for the microtubule experiment (Figure 2), the actin cytoskeleton remained fully developed (Figure 3), no matter whether the more concentrated 1:5 dilution (Figure 3B), or the 1:10 dilution (Figure 3C) were used. These observations were consistent with the quantification results (Figure S10). However, there was an effect of the treatment: as compared to the solvent control (Figure 3A), actin filaments appeared more bundled. However, they retained their full integrity, which contrasts with the thorough elimination observed for microtubules observed for the same treatments, and even for much earlier time points (Figure 2). Thus, MR-1 does not cause a generic breakdown of the cytoskeleton, but is specific for microtubules.

Since fraction MR-1 targeted to microtubules and, therefore, might induce mitotic arrest followed by programmed cell death, potential mortality induced by two dilutions from fraction of MR-1 was scored for 6, 12 and 24 h using the Evans Blue dye exclusion test in tobacco BY-2 cells. Since only a limited amount of the fraction was available, and since mortality scoring requires a larger suspension volume, the dilutions had to be increased (1:200 and 1:1,000, respectively) as compared to the microscope tests. Even so, the more concentrated dilution of 1:200 dilution required 24 h to induce a moderate mortality of around 30% (Figure 4). Thus, there seems to be no acute cytotoxicity, but the slow progression of mortality over 1 d is consistent with a working hypothesis, where mortality is caused by mitotic arrest, since the doubling time of BY-2 cells is in the range of 1 d (Rajabi et al., 2017).

UHPLC-HRMS analysis for identification of main constituents in fraction MR-1

MR-1, the most polar fraction obtained by extraction of *I. tinctoria* roots with MeOH/H₂O 8:2, showed the strongest activity against microtubules (Figures 1, 2). Due to the complexity of the sample and the low amounts available, the MR-1 fraction was investigated by UHPLC(-) electrospray ionization (ESI)-HRMS and MS/MS (Figure 5). The resulting data revealed the presence of 16 compounds (Table S4). Since epigoitrin ((R)-goitrin,

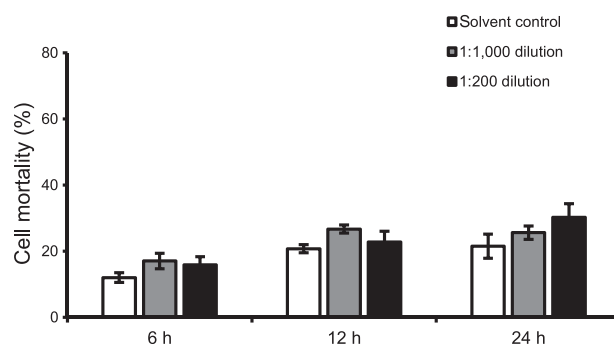


Figure 4. Time course of cell mortality in response to dilutions of fraction MR-1

The relative frequency of dead cells after treatment with MR-1 as compared to control (white bars) in *Nicotiana tabacum* L. cv Bright Yellow 2 (BY-2) was followed over time scoring samples of 1 500 cells for each data point. Data represent three independent biological replicates.

(R)-5-vinylloxazolidine-2-thione) and goitrin ((S)-goitrin, (S)-5-vinylloxazolidine-2-thione) have been described as markers of antiviral efficacy in *I. radix* (Ban Lan Gen) in the *Chinese Pharmacopoeia* 2015 (Dan et al., 2016), their commercially available glucosinolate precursors epigoitrin (allylic glucosinolate), progoitrin (allylic glucosinolate), and, glucobrassicin (indolic glucosinolate) were selected and considered in more detail as potential candidates for the anti-microtubule activity. Also, indirubin, a potential anticancer component of *I. tinctoria*, proposed to bind to tubulin or inhibit several kinases involved in cell division and exerting antimitotic functions against HeLa cells (Mohan et al., 2018), was included into further analysis.

Glucobrassicin exerts anti-microtubule activity

To find out which component of fraction MR-1 is responsible for the anti-microtubule effect, we assessed the response of BY-2 TuA3 cells to standard compounds of epigoitrin, progoitrin, glucobrassicin, and indirubin in a concentration of 50 μ mol/L after 60 min. Upon visualization of microtubules using spinning-

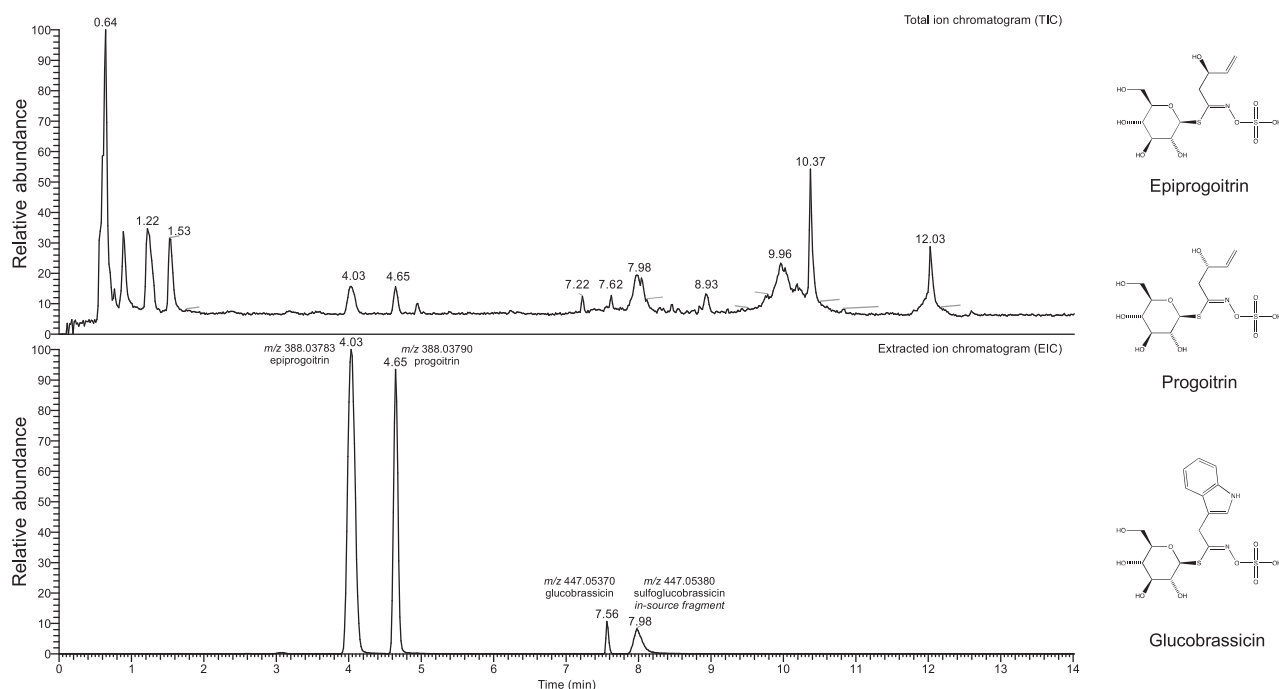


Figure 5. Ultra-high-performance liquid chromatography electrospray ionization high-resolution mass spectrometry (HPLC(-) ESI-HRMS) of fraction MR-1 obtained from *I. tinctoria* root extraction with MeOH/H₂O 8:2

The total ion chromatogram (TIC) is shown on the top, the extracted ion chromatogram (EIC of theoretical [M-H]⁻ ions) of epiprogoitrin (C₁₁H₁₉NO₁₀S₂), progoitrin (C₁₁H₁₉NO₁₀S₂), and glucobrassicin (C₁₆H₂₀N₂O₉S₂) on the bottom.

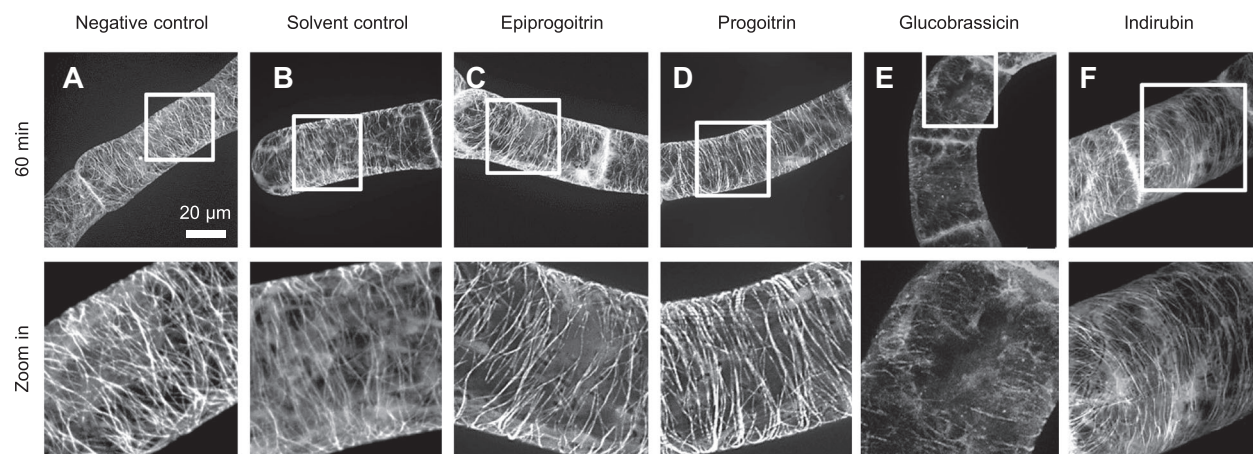


Figure 6. Appearance of microtubules in the microtubule marker line *Nicotiana tabacum* L. cv Bright Yellow 2 α -tubulin-3 green fluorescent protein (BY-2 TuA3-GFP) prior to treatment (A), in response to the solvent (1% dimethyl sulfoxide; B), epiprogoitrin (50 μ mol/L; C), progoitrin (50 μ mol/L; D), glucobrassicin (50 μ mol/L; E), and indirubin (50 μ mol/L; F) after 60 min of treatment observed by spinning-disc microscopy

Geometrical projections from z-stacks collected intervals of 0.5 μ m are shown. Lower row shows zoom-ins of the region marked by the white box in the upper row.

disc microscopy (Figure 6), glucobrassicin clearly stuck out, because it strongly eliminated microtubules accompanied by an increase of diffuse fluorescence in the cytoplasm (Figure 6E). In contrast, neither epiprogoitrin, nor progoitrin produced any effect exceeding that seen for the solvent control (compare Figure 6C, D to Figure 6B). Likewise, there was no obvious difference between solvent control and indirubin treatment

(compare Figure 6E to Figure 6B). The quantification of microtubule integrity indicated that only glucobrassicin induced significant microtubule responses (Figure S11). We tested, whether a combination of 50 μ mol/L epiprogoitrin and progoitrin was able to eliminate microtubules, but observed only a mild effect, manifest as increased diffuse background fluorescence if compared to the solvent control (Figure S12A, B). If

we raised the concentration to 500 $\mu\text{mol/L}$ for epiprogoitrin, progoitrin, or indirubin, we evoked an obvious elimination of microtubules for epiprogoitrin, but not for progoitrin (Figure S12C, B). Likewise, 500 $\mu\text{mol/L}$ of indirubin were not effective in eliminating microtubules (Figure S12D). Further, an exemplary time course of microtubule responses for glucobrassicin was observed and checked in the treatments of 30, 60, 120 and 180 min treatment. The results showed that the integrity of microtubules continued to decline with time (compare Figure 7E to Figure 7B). After 120 min, the microtubule network almost disappeared (Figure 7D, F). Thus, glucobrassicin exerts a specific and clear anti-microtubular activity, which is not seen in any of the other compounds tested.

If glucobrassicin would act on microtubule-associated proteins that differ fundamentally between plant and animal cells, it should not affect microtubules in mammalian cells. We followed, therefore, the response of HeLa cells expressing a GFP-tubulin marker to 50 $\mu\text{mol/L}$ of glucobrassicin over 90 min (Figure 8), but also assessed the cellular response after 1 d (Figure 9). Microtubules were strongly affected already at 30 min after addition of glucobrassicin (Figure 8C) and even after 90 min had still not

returned to the situation seen in the solvent control (Figure 8A, B). In agreement with our observations, the quantification results also revealed that glucobrassicin significantly reduced microtubule integrity (Figure S13). In addition, after treatment with 25 $\mu\text{mol/L}$ of glucobrassicin after 24 h, many cells were found to have entered apoptosis, which was even more advanced as that induced by 1 $\mu\text{mol/L}$ colchicine, used as a positive control (Figure 9). Thus, the anti-microtubular effect of glucobrassicin was confirmed in HeLa cells as well, and this was followed by a drastic apoptosis in these mammalian cells.

Since glucobrassicin showed anti-microtubular effects, and therefore, might reduce the cell division via inducing mitotic arrest, we scored the mitotic index of BY-2 TuA3-GFP cells, and also quantified the incidence of different mitotic microtubule arrays reporting the progression of mitosis. In the control, we could find one to two mitotic cells in any image, but in the glucobrassicin sample usually none. There was also the impression that the treated cells were wider (Figure 10A, E). The cortical microtubules in the control were clearly visible, although there was some soluble pool in the cytoplasm, which is typical for cells in G_2 (cortical MTs disappear with appearance of the prophase

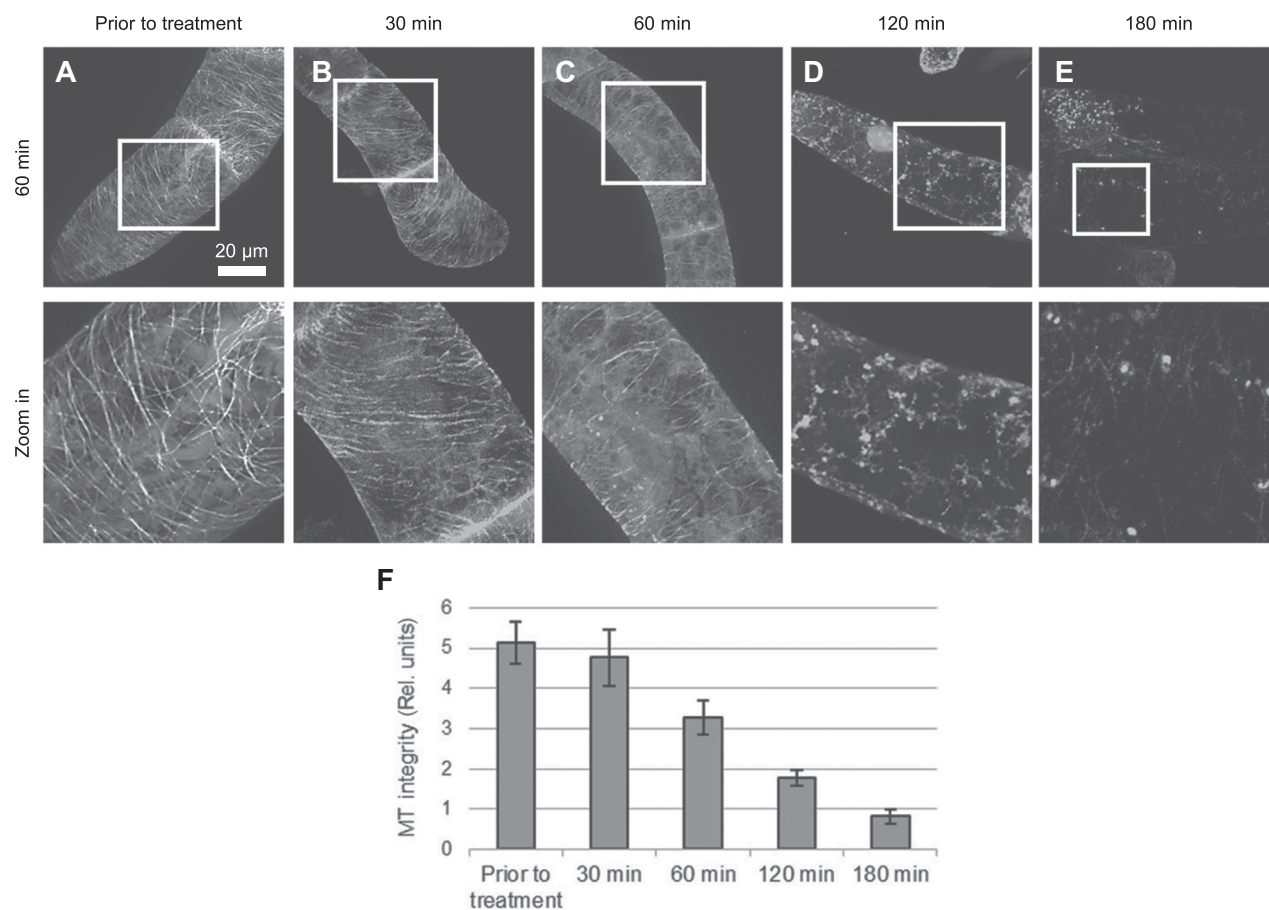


Figure 7. Exemplary time course of microtubule responses for glucobrassicin in the microtubule marker line *Nicotiana tabacum* L. cv Bright Yellow 2 α -tubulin-3 green fluorescent protein (BY-2 TuA3-GFP)

The cellular microtubule prior to treatment (A), and in response to 50 $\mu\text{mol/L}$ glucobrassicin treatment in a time course of 30 min (B), 60 min (C), 120 min (D), and 180 min (E) were observed by spinning-disc microscopy. Geometrical projections from z-stacks collected at intervals of 0.5 μm are shown. Lower row shows zoom-ins of the region marked by the white box in the upper row. (F) Quantification of microtubule integrity for the glucobrassicin in different time points.

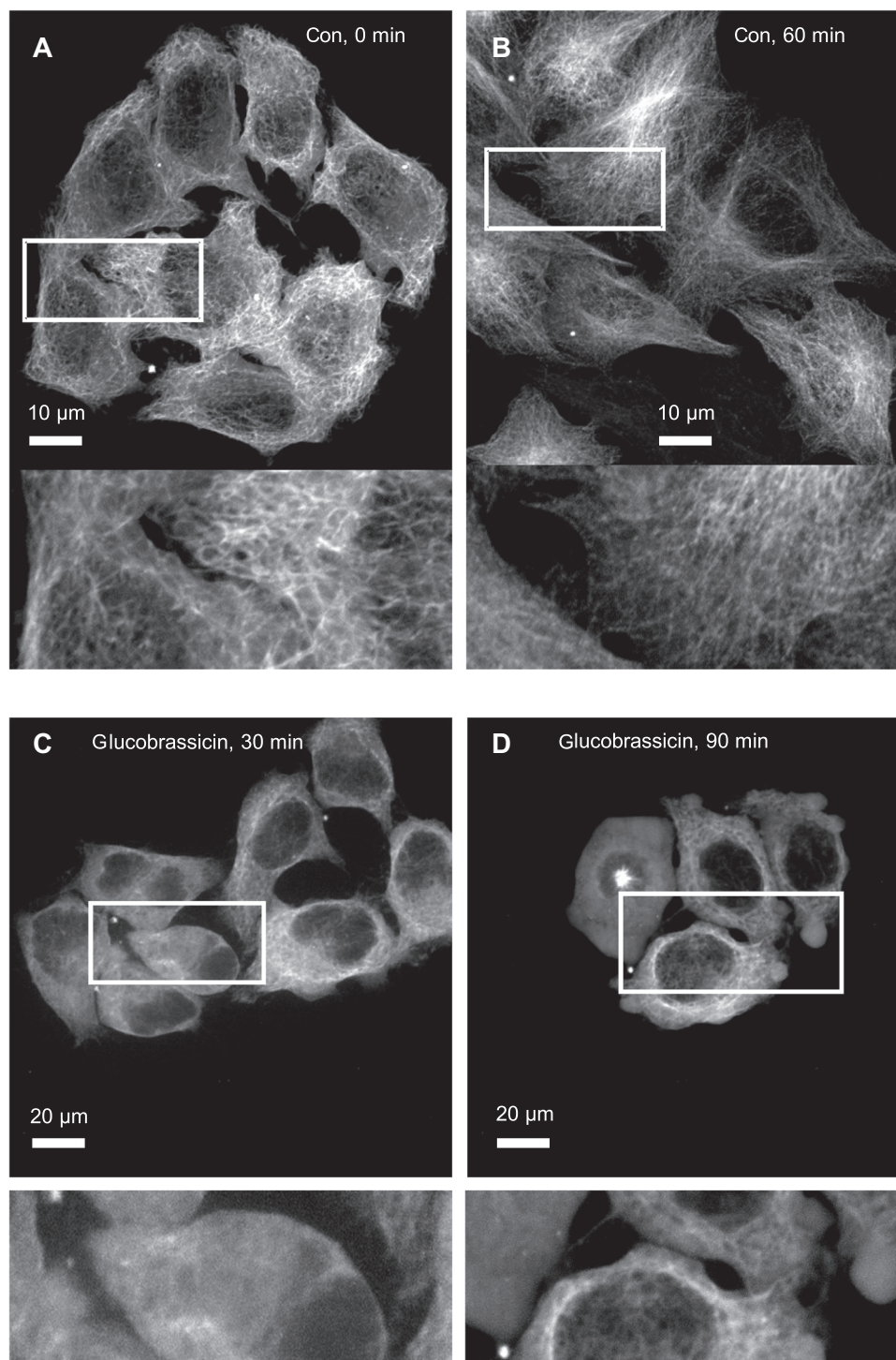


Figure 8. Exemplary time course of microtubule responses for glucobrassicin in HeLa cells expressing a green fluorescent protein (GFP)-tubulin marker

The cellular microtubule of control treatment 0 min (A) and 60 min (B), and in response to 50 $\mu\text{mol/L}$ glucobrassicin in an exemplary time course of 30 min (C), 90 min (D) were observed by spinning-disc microscopy. Geometrical projections from z-stacks collected at intervals of 0.5 μm are shown. Lower row shows zoom-ins of the region marked by the white box in the upper row.

band and return only after telophase) (Figure 10B). In contrast, in the treated cells, microtubules were mostly gone, only a few residual microtubules persisted (Figure 10F). The spindle in the control shows the usual kinetochor fibers (Figure 10C). In treated

cells, spindles were not only very rare (around 1/10 of the frequency seen in the control), but they also lacked internal structure and were also not as bright (Figure 10G). Phragmoplasts were common in the control and looked normal (Figure 10B).

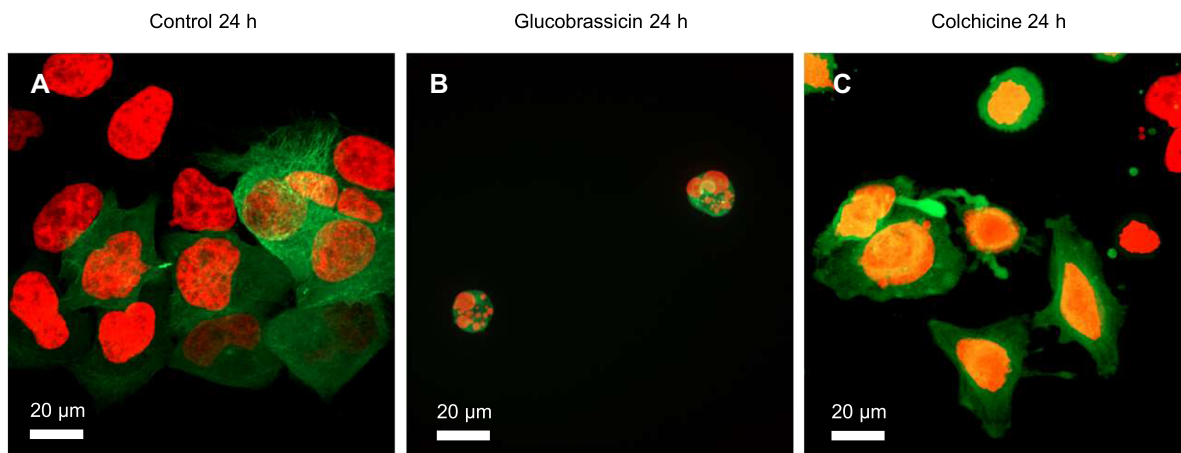


Figure 9. Apoptosis of HeLa cells expressing a green fluorescent protein (GFP)-tubulin marker in response to glucobrassicin and colchicine
(A) Control treatment for 24 h; **(B)** 25 μmol/L glucobrassicin treatment for 24 h; **(C)** 1 μmol/L colchicine treatment for 24 h.

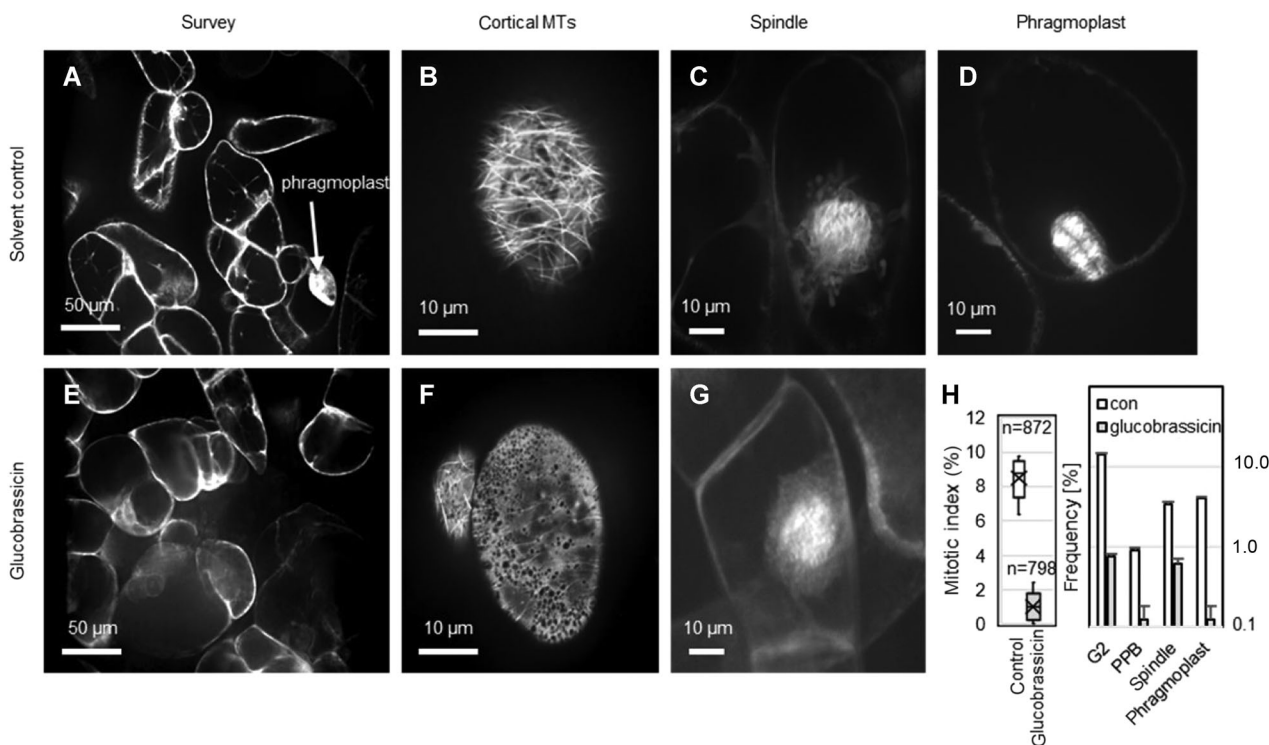


Figure 10. Changes in the mitotic index of Bright Yellow 2 α -tubulin-3 green fluorescent protein (BY-2 TuA3-GFP) cells after glucobrassicin treatment

Two typical surveys were shown in the treatment of solvent control **(A)** and glucobrassicin **(E)**. Exemplary cell of cortical microtubules (MTs) **(B)**, spindle **(C)**, and phragmoplast **(D)** for the solvent control are shown in the upper panels. The corresponding responses of cortical MTs **(F)**, and spindle **(G)** for glucobrassicin are shown in lower panels. The changes of mitotic index and frequency of cells in different division stages for glucobrassicin are given.

However, in the treated samples, we hardly could spot a single phragmoplast. When we quantified the changes, we found that glucobrassicin reduced the mitotic index drastically, by a factor of >4 (Figure 10H). As a consequence, in the treated cells, the frequency of each division stage was lower than that of control, but to a different extent (Figure 10H). While spindles were still present, albeit more scarcely, the suppression of preprophase

bands and phragmoplasts was far more drastic. Moreover, cells in G₂ were also much rarer than in the solvent control. Since glucobrassicin obviously can impair mitosis, we wondered whether this mitotic arrest would culminate in programmed cell death.

Therefore, BY-2 cells were treated with 50 μmol/L epiprogoitrin, 50 μmol/L progoitrin, 50 μmol/L glucobrassicin,

and 50 $\mu\text{mol/L}$ indirubin for 24 h. The results revealed that none of these compounds induced any significant mortality, such that they seem not to be responsible for the mortality induced by fraction MR-1 caused mortality (Figure S14).

DISCUSSION

Plant secondary metabolism is very rich, which is possibly linked to the fact that plants as sessile organisms have to rely on chemical manipulation of other organisms to ensure their survival. Therefore, many plant compounds exert also a medical effect and have been a valuable source of therapeutic products through history and at the present (for reviews see Atanasov et al., 2015; Newman and Cragg, 2020). Traditional systems of healing are often centered on medicinal plants. However, even for elaborate phytotherapeutical systems, such as TCM, the molecular modes of actions have remained elusive, which limits their use in modern evidence-based medicine. In the current work, we exemplarily address the mode of action of Northern Ban Lan (*I. tinctoria*), a plant traditionally used to cure viral and tumor diseases (for a recent review see Kaul et al., 2019), currently attracting considerable interest due to its effect against Covid-19 (reviewed in Yang et al., 2020). Using a fluorescently tagged plant cell line, we demonstrate that extracts from this plant exert anti-microtubular activity. Using bioactivity-guided HPLC fractionation, we identify glucobrassicin as candidate compound accounting for this anti-microtubular activity. In the following, we discuss the analytical evidence for the identification of the active compound, and the biological context of its genesis. Then, we consider the question, to what extent the anti-microtubular effect is specific and how it can account for the observed medical effect, before considering the therapeutical potential of our discovery.

What is the analytical evidence for glucobrassicin?

Based on currently available data about the composition of *I. tinctoria* plant extracts (see introduction), it was decided to adapt the methodology of Glauser et al. (2012) for the UHPLC-(−)ESI-HRMS analysis of fraction MR-1. A charge surface hybrid (CSH) HPLC column was selected, providing high loading of basic compounds and undistorted peak shapes with modifiers of low ionic strength, such as formic acid (Lauber et al., 2013). These properties are essential for the analysis of complex samples obtained from plants containing metabolites of different polarities. As polar compounds were expected to be active, we employed a very narrow gradient to allow for the best chromatographic resolution and a good quality of MS/MS data. Preliminary UHPLC-HRMS analysis of the polar regions of the chromatogram quickly revealed the presence of remarkable isotopic patterns featured an increased abundance in the peak X + 2, most probably attributed to a presence of sulfur atoms. Calculation of the molecular formulas indeed revealed $\text{C}_{11}\text{H}_{18}\text{NO}_{10}\text{S}_2$ at t_R 4.03 min (m/z 388.03783, 0.18 ppm, $[\text{M}-\text{H}]^-$) and t_R 4.65 min (m/z 388.03790, 0.36 ppm, $[\text{M}-\text{H}]^-$),

accompanied by $\text{C}_{16}\text{H}_{19}\text{O}_9\text{N}_2\text{S}_2$ (m/z 447.05370, −0.10 ppm, $[\text{M}-\text{H}]^-$) at t_R 7.65, and $\text{C}_{16}\text{H}_{19}\text{O}_9\text{N}_2\text{S}_2$ (m/z 447.05380, −0.12 ppm, $[\text{M}-\text{H}]^-$) at t_R 7.98; see Figure 5). Subsequent chromatogram deconvolution and MS/MS matching with public datasets revealed that these masses corresponded to the glucosinolates progoitrin, epi-progoitrin, glucobrassicin, and the in-source MS fragment $[\text{M}-\text{HSO}_3]^-$ of sulfoglucobrassicin, respectively (Table S4). The MS/MS data coincided well with the literature, featuring all diagnostic fragments with comparable intensities (Cataldi et al., 2007). Unfortunately, it was impossible to unambiguously assign both isomers progoitrin and its epimer epiprogoitrin, as both produced similar fragmentation spectra. For this reason, we used a published elution order obtained under similar chromatographic conditions (Mohn et al., 2007). We focused on fraction MR-1 as the most promising fraction. In addition, epiprogoitrin additional constituents were reliably identified in fraction MR-1 as listed in Table S4. This does not exclude additional compounds with anti-microtubular activity in leaves, but was just a necessary prioritization.

Allylic or indolic glucosinolates such as progoitrin and epiprogoitrin or glucobrassicin derivatives (Figure 5) qualified as good candidates for bioactivity. For example, glucobrassicin can be found in most species of Brassicaceae such as broccoli, cabbages and woad (reviewed in Fahey et al., 2001). Related compounds, such as sulfoglucobrassicin, 1-methoxyglucobrassicin, 4-hydroxyglucobrassicin, and 4-methoxyglucobrassicin also belong to the most common secondary metabolites in this family. These compounds accumulate in response to herbivory (Agerbirk et al., 2009). Indole glucosinolates derive from tryptophan secondary metabolism. Tryptophan is first converted to indole-3-acetaldoxime (IAOx) by the cytochrome P_{450} enzymes CYP79B2 and CYP79B3. Another CYP₄₅₀ enzyme, CYP83B1, catalyzes the transition from IAOx to the intermediate 1-acetylthio-2-indolyl-ethane, which is then giving rise to a S-alkylthio-hydroximate derivative. This intermediate incorporates a thiol moiety from the C-S lyase SUR1, and a final glycosylation step through the glucosyltransferase UGT74B1 (Bender and Celenza, 2009) leads then to the product indol-3-ylmethyl-desulfoglucosinolate (glucobrassicin).

The bioactivity of these compounds is supported by epidemiological studies showing that the indole glucosinolates reduce the risk of lung, stomach, colon and rectal cancer (Verhoeven et al., 1996). Glucobrassicin, in particular, is converted, upon chewing vegetables, to indole-3-carbinol (I3C), which then undergoes condensation to 3,3'-diindolymethane (DIM) in the acidic conditions upon digestion in the stomach. Both compounds have attracted considerable attention in the context of cancer prevention (Katz et al., 2018). The mode of action for I3C seems to be the induction of specific autophagocytic events, possibly by binding to elastase, preventing a cancer-associated modification of the cell-cycle regulator cyclin E and the cleavage of CD40, a member of the tumor necrosis factor family. Furthermore, isothiocyanates (ITCs), deriving from the degradation of glucosinolates, induce apoptosis in bladder cancer cells and microtubule breakdown

at concentrations around 10 $\mu\text{mol/L}$ (Øverby et al., 2015). For lung cancer cells, these compounds were shown to bind to tubulin and to recruit both α - and β -tubulin for degradation in the proteasome (Mi et al., 2009).

For what purpose is *I. tinctoria* accumulating anti-microtubular compounds?

So far, three ideas on the potential function of glucobrassicin derivatives have been proposed. The discovery that glucobrassicin can induce curvatures in the *Avena* coleoptile assay (Andersen and Muir, 1966), stimulated the idea that it might represent a storage form, from which auxin can be readily mobilized upon need (Kefeli et al., 1970). Alternatively, the invasive character of *I. tinctoria* along with the herbicidal activity of processed leaves led to the idea that it might act as an allelopathic compound (Brown and Morra, 1995). For instance, glucobrassicin has been isolated from the leaves of *I. tinctoria* (Mohn et al., 2009). Since glucosinolates always occur in concert with a myrosinase that becomes active upon tissue damage, it might act against herbivores (Elliott and Stowe, 1971). To resolve the biological function of a compound it is useful to consider the conditions under which it accumulates. In fact, glucobrassicins in *Isatis* accumulate in response to jasmonic acid, but also wounding (Galletti et al., 2006; Karakaş, 2019), clearly supporting a role in warding off herbivores. Actually, the name goitrin derives from the ability of these compounds to induce human goiters through the milk from cows that feed on Brassicaceae (Michajlovskij et al., 1970). Thus, the most likely hypothesis for the functional context of glucobrassicin accumulation is that *Isatis* produces anti-microtubule compounds as defense against herbivory. Since glucobrassicin can affect microtubules in HeLa cells (Figure 8), this anti-microtubular activity is probably affecting tubulins themselves rather than acting on microtubule-associated proteins that differ fundamentally between plant and animal cells. The strategy to poison the microtubular cytoskeleton of the herbivore is not uncommon in plants. For instance, citral, a compound that can disrupt microtubules (Chaimovitch et al., 2010) is released from lemongrass and can impair larval development of herbivorous insects (Brügger et al., 2019). Madagascar periwinkle (*Catharanthus roseus*) activates anti-microtubular vinca alkaloids in response to caterpillar attack (de Bernonville et al., 2017).

Viral interaction of microtubules as drug target

The antiviral properties (for review see Hamburger, 2002) of *I. tinctoria* preparations might derive from the anti-microtubular activity demonstrated in our study. Infection of influenza viruses involves receptor-mediated endocytosis, slow movement along cortical actin filaments, and then transfer to microtubules that are usurped for long-distance transport as “superhighways” to reach the perinuclear region and to enter the nucleus for replication (Liu et al., 2012, 2014; Banerjee et al., 2013; Zhang et al., 2018). Thus, the microtubules of the host cell are hijacked for directional intracellular transport, viral shell disassembly, and genome release. The microtubule network remodels under the influence of

modulating lysine deacetylases (for a recent review see Simpson and Yamauchi, 2020). The elimination of microtubules by specific fractions of *I. tinctoria* extracts and by glucobrassicin would interfere with this mechanism for viral spread. In fact, studies of viral colonization in cell cultures show that disruption of microtubules affects colonization success (reviewed in Naghavi and Walsh, 2017). This mechanism seems to be conserved across eukaryotic kingdoms, since also many plant viruses use microtubules as track for movement, possibly making use of microtubule treadmilling. In fact, when treadmilling of microtubules was reduced by genetic manipulation, this slowed down the spread of tobacco mosaic virus in tobacco (Ouko et al., 2010).

Outlook: toward evidence-based use of Northern Ban Lan

Traditional Chinese Medicine represents a rich body of phytotherapeutic activities that have been elaborated and validated over several millennia. Nevertheless, outside of China, the acceptance of this system of healing has met certain reservations. One of the central limitations is that molecular explanations for the empirical record are often absent. Instead, the activities are described by relatively vague phenomenological terms, such as “anti-inflammatory”, “antiviral”, “anticancer”, or “invigorating”. To develop the medical potential for this rich body of phytotherapeutic activities, a mechanistic understanding is mandatory. Our discovery that extracts from *I. tinctoria* (Northern Ban Lan) eliminate microtubules and that this activity can be attributed to glucobrassicin, opens a new possibility to understand the antiviral activity by testing implications of the hypothesis that the target of glucobrassicin is microtubule-driven transport of viral particles. We would predict, for instance, that the spread of fluorescently labeled viral particles in a cellular system should slow down in presence of glucobrassicin (Ouko et al., 2010), or that the affinity of tubulin for binding compounds could be outcompeted by glucobrassicin (Wiesler et al., 2002). Last, but not least, it would be interesting to test whether boosting glucobrassicin contents in Ban Lan Gen by agricultural or processing practices, such as controlled wounding, might improve its therapeutical effect.

MATERIALS AND METHODS

Cell lines and cell cultivation

To observe microtubules, a tobacco BY-2 (*Nicotiana tabacum* L. cv Bright Yellow 2) suspension cell line stably expressing tobacco TuA3 fused to GFP was used (Hohenberger et al., 2011). Actin filaments were followed in the marker line BY-2 GF11, expressing the actin-binding domain 2 of plant fimbrin in fusion with GFP (Sano et al., 2005). In some experiments, non-transformed tobacco BY-2 (wild type (WT)) cells were used as control. The cells were cultivated in liquid medium containing 4.3 g/L Murashige and Skoog salts, 30 g/L sucrose, 200 mg/L KH_2PO_4 , 100 mg/L inositol, 1 mg/L thiamine, and 0.2 mg/L 2,4-dichlorophenoxyacetic acid (2,4-D),

adjusted to pH 5.8. Transgenic cells were supplemented with the respective antibiotics (50 mg/L kanamycin in case of the BY-2 TuB3 cell line, 30 mg/L hygromycin in case of BY-2 GF11 cell line). The WT and BY-2 GF11 cells were subcultured weekly by inoculating 1.5 mL of stationary cells into 30 mL of fresh, autoclaved liquid medium in 100 mL Erlenmeyer flasks. The BY-2 TuA3 cells were subcultured in the same way, but only every 14 d, since they were proliferating more slowly. All cell suspensions were incubated at 25°C in the dark on an orbital shaker at 150 rpm.

HeLa Kyoto cells with enhanced GFP-tagged α -tubulin and H2B-mCherry chromatin marker were cultured in Dulbecco's modified Eagle's medium + GlutaMax-I (ThermoFisher) supplemented with 10% fetal bovine serum (Capricorn Scientific) and 1% penicillin/streptomycin (Capricorn Scientific) at 37°C and 5% CO₂ (Schmitz et al., 2010). The day before the experiment, a 12-well plate with coverslips was prepared and 1 mL of culture medium containing approximately 1×10^5 cells was added to each well. The cells were cultured overnight at 37°C and 5% CO₂.

I. tinctoria extraction and fractionation

Dried plant material was ground to a fine powder using a grind mill (5 SS beads; RETSCH 400MM), then extracted with either MeOH/H₂O (8:2), or with ethyl acetate (EtOAc, 5 mL/200 mg leaves and 10 mL/1000 mg roots), respectively in an ultrasonic bath (30 min for leaves/60 min for roots, 30°C) using glassware exclusively. The extract was cleared by centrifugation, and the solvent of the liquid phase either evaporated under N₂ or lyophilized to obtain the dry crude extracts (yields are summarized in Table S1).

The solutions used for fractionation were prepared as follows: the dry extracts were first reconstituted with pure MeOH, and filtered through a 0.2 μ m polytetrafluorethylene filter. The saturated supernatants were then transferred to 2 mL glass vials, and dried under N₂. After determining their weight, they were finally reconstituted with the original volume of MeOH.

Crude extracts were fractionated on a semi-preparative HPLC system, consisting of two LC20-AP solvent delivery units, a SPD-20A UV/Vis detector equipped with an analytical UV cell, a CBM-20A control module, and an FRC-10A fraction collector (Shimadzu Corporation, Kyoto, Japan). An Uptisphere® UP3HDO-15QS (4.6 \times 150 mm, 3 μ m, 120 Å; Interchim, Montluçon, France) analytical column was employed for all separations at room temperature. The mobile phase consisted of H₂O + 0.1% v/v HCOOH (A) and CH₃CN + 0.1% v/v HCOOH (B) at a flow rate of 1 mL/min. Gradient profiles used for the fractionation of each extract are summarized in Table S2. The UV/Vis responses were recorded at 254 and 280 nm. The fractions were collected automatically at 3.5 min intervals.

After consecutive separation of the crude extracts, the corresponding fractions were pooled and evaporated to dryness under nitrogen at room temperature to obtain the 54 samples ML-1 to ML-12, EL-1 to EL-14, MR-1 to MR-14, and ER-1 to ER-14 used for bioactivity tests and structure elucidation (Table S3).

Live-cell imaging

The response of microtubules was followed over time making use of the GFP-labeled tobacco TuA3 in individual cells by spinning-disc confocal microscopy. To screen candidate fractions, the 54 fractions were reconstituted with 10 μ L dimethyl sulfoxide (DMSO) and subsequently diluted with 40 μ L ultra-pure water for their effect on cells in the proliferation phase (4–10 d after subculture) by adding 5 μ L of the fraction into an aliquot of 100 μ L cell suspension in a reaction tube, and mixing gently at 25°C in the dark on an orbital shaker at 150 rpm for 1 h. As a solvent control, 100 μ L of cell suspension were treated with the solvent (1% DMSO). The microtubule-eliminating herbicide oryzalin (10 μ mol/L) (Sigma-Aldrich, Deisenhofen, Germany) was used as a positive control. For the time course experiments, the cells were observed by microscopy directly after addition of the dissolved fraction.

To see the effect of candidate compounds, either glucobrassicin (50 μ mol/L), epiprogoitrin (50 and 500 μ mol/L), progoitrin (50 and 500 μ mol/L), an equimolar combination of epiprogoitrin and progoitrin (50 μ mol/L), or indirubin (50 and 500 μ mol/L) were tested for their effect on microtubules in the TuA3 cell line. The response of mitosis to 50 μ mol/L glucobrassicin was monitored in BY-2 TuA3-GFP cells by constructing frequency distributions of different mitotic stages (visible from microtubular organization) and determining the mitotic index integrating over mitotic stages in relation to the entire cell population. The sampling was conducted by spinning-disc confocal microscopy at low magnification (25 \times objective). Data represent a population of around 800 individual cells collected from three independent experiments.

The tested pure compounds, that is, glucobrassicin, epiprogoitrin, progoitrin, and indirubin, were obtained from Sigma-Aldrich (Deisenhofen, Germany).

To obtain insight into the specificity of the bioactive fraction MR-1 from root extracts, the effect on actin filaments was assessed as well in some of the experiments, making use of the marker line GF11, again using spinning-disc confocal microscopy. Again, the cells were used in the exponential phase (4 d after subculture).

Microtubule responses in HeLa cells were assayed after treatments with 50 μ mol/L glucobrassicin for 30 and 90 min in the enhanced GFP- α -tubulin/H2B-mCherry cell line. Apoptosis was analyzed after 24 h of treatment with either 50 μ mol/L glucobrassicin or 1 μ mol/L colchicine (as a positive control; Sigma-Aldrich) by spinning-disc confocal microscopy.

Confocal images were recorded with an AxioObserver Z1 using a 63 \times LCI-NeofluarImmCorr DIC objective (NA 1.3), the 488-nm emission line of an Ar-Kr laser, and a spinning-disc device (YOKOGAWA CSU-X1 5000). At different time points after onset of the treatment, z-stacks were captured and processed using ZEN software (Zeiss, Jena) to generate orthogonal projections from the recorded stacks and to export them in TIFF format.

Quantitative image analysis

Microtubule integrity was quantified using the freeware ImageJ (<https://imagej.net>) based on a method modified from Schwarzerová et al. (2002). In short, we collected four intensity profiles along the elongation axis equally spaced over the cross axis (using the shortcut Ctrl+K), setting the width of the probing line to 25 pixels to compensate for local random fluctuations of intensity. Subsequently, these profiles were imported into a preset Excel sheet to calculate the first derivative at each position of the profile. In the rising flank of a microtubule intersected by the profile, this value would be positive, in the trailing flank, it would be negative. To eliminate thermal noise from the photomultiplier, subsequent values along the profile were added, and the absolute value of the sum was recorded. A random signal of a single pixel should lead to a value of zero and, thus, not contribute to the quantification. The SD over these filtered first derivatives increases proportionally with the integrity of microtubules. To calibrate for potential differences in laser intensity between different measurements, the SD was normalized to the maximal intensity within the profile of three images.

The density of actin filaments was also quantified by ImageJ based on methods modified from Schwarzerová et al. (2002) and Guan et al. (2020).

Cell mortality assay

Mortality was determined using the Evans Blue assay (Gaff and Okong'O-Ogola, 1971). As membrane-impermeable dye, Evans blue can only stain the cytoplasm of dead cells, where the integrity of the plasma membrane has been lost. Living cells will not be stained. Mortality can then be scored as relative frequency of blue cells. At least 1,500 cells were scored per sample.

Mortality of non-transformed (WT) BY-2 cells was determined in response to fraction MR-1 (diluted 1:200 or 1:1 000), or to 50 $\mu\text{mol/L}$ of either epiprogoitrin, progoitrin, glucobrassicin, or indirubin for the indicated time intervals. These measurements were accompanied by appropriate solvent controls (1% or 0.1% DMSO). Aliquots of 300 μL of cell suspension per sample were transferred into custom-made staining chambers (Nick et al., 2000) to remove the medium. The cells were incubated in 2.5% (w/v) Evans Blue for 3 min, and washed two times with distilled water. About 40 μL of the stained cells were transferred onto the microscopic slide and imaged using an AxioImager Z.1 microscope. At least 500 cells were scored manually per sample. Data represent three independent biological replicates with at least 500 individual cells per replicate.

Significance of observed differences was tested using an unpaired Student's *t*-test.

UHPLC-HRMS/MS

Samples for UHPLC-HRMS analysis were prepared from the residues of two HPLC fractionation runs that were reconstituted with MeOH (750 μL per run), pooled, evaporated to

dryness under a gentle N_2 stream at ambient temperature, and reconstituted with 100 μL of MeOH.

Chromatographic separations were performed on a Dionex UltiMate 3000 UHPLC system (Thermo Fisher Scientific, USA), equipped with a CTC PAL autosampler, an UV/Vis diode array detector (DAD), a heated column compartment, and a solvent delivery system. The UV1 channel was set to 254 nm, the UV2 channel to 280 nm. The DAD detection range was between 200 and 800 nm at a data collection rate of 5 Hz. The components of the active fraction MR-1 (1 μL) were separated on a Waters Acquity® CSH C_{18} column (2.1 \times 100 mm, 1.8 μm particle size) at a flow rate of 0.45 mL/min using the following linear gradient (expressed as % solvent B): 2% for 3 min, increase to 20% between 3 and 6 min, then to 100% between 6 and 9 min, 100% between 9 and 11 min, and final equilibration at 2% between 11 and 14 min. The mobile phase consisted of H_2O + 0.1% v/v HCOOH (A) and CH_3CN + 0.1% v/v HCOOH (B). The temperature of the column compartment was maintained at 30°C.

The UHPLC system was coupled with a QExactive orbitrap mass spectrometer (Thermo Fisher Scientific), equipped with a heated ESI source and supplied with N_2 as a collision gas. The default ion source settings for the above specified flow rate were applied. Data were acquired in the negative ionization mode, at 35,000 full-width half-maximum resolution (FWHM), in a scan range between 50 and 750 m/z , with an automatic gain control (AGC) target of 3×10^6 , and a maximal injection time of 100 ms. MS/MS experiments were conducted at 17,500 resolution in the data-dependent mode (five top peaks as precursors for each full scan spectrum) with a normalized collision energy of 30 eV. The AGC target was set to 8×10^3 for a maximal injection time of 50 ms. Precursor ions were selected at an intensity threshold of 1.5×10^5 , with enabled isotope exclusion, and dynamic exclusion of 2.5 s. Mass accuracy was calibrated below 2 ppm using the Pierce® LTQ Velos calibration solution according to the requirements of the manufacturer.

The collected MS/MS data were de-convolved with the MS-DIAL software package (ver. 4.16; Tsugawa et al., 2015) making use of publicly available MS/MS datasets (>30,000 records). The mass accuracy tolerance in MS and MS/MS mode was set to a threshold of 5 mDa, mass slice width to 10 mDa, and the threshold amplitude to 10^5 counts. Identification score threshold of 90% was required for matching. Molecular formula calculation under consideration of isotopic pattern was provided by FreeStyle software (ver. 1.6; Thermo Fisher Scientific).

ACKNOWLEDGEMENTS

We thank the team of Prof. Dr. Sylvia Erhardt (Zoological Institute of the KIT), especially MSc Agnieszka Pancholi for their help with the experiments on the HeLa cells. This work was supported by fellowships from the China Scholarship Council to Pingyin Guan to Xin Zhu and Kunxi Zhang.

CONFLICT OF INTERESTS

The authors declare they have no conflicts of interest.

AUTHOR CONTRIBUTIONS

P.N., L.B., and Q.W.-M. conceived the original research plan and revised the manuscript; P.G., J.Z., S.G., X.Z., M.S., and K.Z. performed the experiments; P.G., J.Z., S.G., X.Z., K.Z., L.B., and P.N. analyzed the data; P.G., J.Z., and S.G. wrote the manuscript. All authors read and approved of its content.

Edited by: Haiyun Ren, Beijing Normal University, China

Received Aug. 2, 2021; **Accepted** Oct. 4, 2021; **Published** Oct. 12, 2021

OO: OnlineOpen

REFERENCES

- Agerbirk, N., Vos, M.D., Kim, J.H., and Jander, G. (2009). Indole glucosinolate breakdown and its biological effects. *Phytochem. Rev.* **8**: 101–120.
- Altmann, K.H., and Gertsch, J. (2007). Anticancer drugs from nature—natural products as a unique source of new microtubule-stabilizing agents. *Nat. Prod. Rep.* **24**: 327–357.
- Andersen, A.S., and Muir, R. (1966). Auxin activity of glucobrassicin. *Plant Physiol.* **19**: 1038–1048.
- Atanasov, A.G., Waltenberger, B., Pferschy-Wenzig, E.M., Linder, T., Wawrosch, C., Uhrin, P., Temml, V., Wang, L., Schwaiger, S., and Heiss, E.H. (2015). Discovery and resupply of pharmacologically active plant-derived natural products: A review. *Biotechnol. Adv.* **33**: 1582–1614.
- Banerjee, I., Yamauchi, Y., Helenius, A., and Horvath, P. (2013). High-content analysis of sequential events during the early phase of influenza A virus infection. *PLoS One.* **8**: e68450.
- Bender, J., and Celenza, J.L. (2009). Indolic glucosinolates at the crossroads of tryptophan metabolism. *Phytochem. Rev.* **8**: 25–37.
- Bernardini, S., Tiezzi, A., Laghezza Masci, V., and Ovidi, E. (2018). Natural products for human health: An historical overview of the drug discovery approaches. *Nat. Prod. Res.* **32**: 1926–1950.
- Brattström, A., Schapowal, A., Kamal, M., Maillet, I., Ryffel, B., and Moser, R. (2010). The plant extract *Isatis tinctoria* L. extract (ITE) inhibits allergen-induced airway inflammation and hyperreactivity in mice. *Phytomedicine* **17**: 551–556.
- Brown, P.D., and Morra, M.J. (1995). Glucosinolate-containing plant tissues as bioherbicides. *J. Agric. Food Chem.* **12**: 3070–3074.
- Brügger, B.P., Martínez, L.C., Plata-Rueda, A., e Castro, B.M.dC., Soares, M.A., Wilcken, C.F., Carvalho, A.G., Serrão, J.E., and Zanuncio, J.C. (2019). Bioactivity of the *Cymbopogon citratus* (Poaceae) essential oil and its terpenoid constituents on the predatory bug, *Podisus nigrispinus* (Heteroptera: Pentatomidae). *Sci. Rep.* **9**: 1–8.
- Cataldi, T.R., Rubino, A., Lelario, F., and Bufo, S.A. (2007). Naturally occurring glucosinolates in plant extracts of rocket salad (*Eruca sativa* L.) identified by liquid chromatography coupled with negative ion electrospray ionization and quadrupole ion-trap mass spectrometry. *Rapid Commun. Mass Spectrom.* **21**: 2374–2388.
- Chaimovitch, D., Abu-Abied, M., Belasov, E., Rubin, B., Dudai, N., and Sadot, E. (2010). Microtubules are an intracellular target of the plant terpene citral. *Plant J.* **61**: 399–408.
- Dan, Y., Qian, Z., Peng, Y., Chen, C., Liu, Y., Tai, W., and Qi, J. (2016). Revision and improvement of criterion on Traditional Chinese Medicines in Chinese Pharmacopoeia 2015. *Chin. Herb. Med.* **8**: 196–208.
- David, B., Wolfender, J.L., and Dias, D.A. (2015). The pharmaceutical industry and natural products: Historical status and new trends. *Phytochem. Rev.* **14**: 299–315.
- de Bernonville, T.D., Carqueijeiro, I., Lanoue, A., Lafontaine, F., Bel, P. S., Liesecke, F., Musset, K., Oudin, A., Glévarec, G., and Pichon, O. (2017). Folivory elicits a strong defense reaction in *Catharanthus roseus*: Metabolomic and transcriptomic analyses reveal distinct local and systemic responses. *Sci. Rep.* **7**: 1–14.
- Demain, A.L., and Vaishnav, P. (2011). Natural products for cancer chemotherapy. *Microb. Biotechnol.* **4**: 687–699.
- Dogterom, M., and Koenderink, G.H. (2019). Actin–microtubule crosstalk in cell biology. *Nat. Rev. Mol. Cell Biol.* **20**: 38–54.
- Dostál, V., and Libusová, L. (2014). Microtubule drugs: Action, selectivity, and resistance across the kingdoms of life. *Protoplasma* **251**: 991–1005.
- Dumontet, C., and Jordan, M.A. (2010). Microtubule-binding agents: A dynamic field of cancer therapeutics. *Nat. Rev. Discov.* **9**: 790–803.
- Elliott, M.C., and Stowe, B.B. (1971). Distribution and variation of indole glucosinolates in woad (*Isatis tinctoria* L.). *Plant Physiol.* **48**: 498–503.
- Fahey, J.W., Zalcmann, A.T., and Talalay, P. (2001). The chemical diversity and distribution of glucosinolates and isothiocyanates among plants. *Phytochemistry* **56**: 5–51.
- Florian, S., and Mitchison, T.J. (2016). Anti-microtubule drugs. In: *Methods in Molecular Biology*. 2nd edn, Vol. 1413. New York: Springer New York. pp. 403–421.
- Forth, S., and Kapoor, T.M. (2017). The mechanics of microtubule networks in cell division. *J. Cell Biol.* **216**: 1525–1531.
- Fredriksson, M. (2017). From biopiracy to bioprospecting: Negotiating the limits of proprietization. *Property, Place and Piracy* (Ch. 15), In: J. Arvanitakis, M. Fredriksson, eds. London: Routledge.
- Gaff, D., and Okong'O-Ogola, O. (1971). The use of non-permeating pigments for testing the survival of cells. *J. Exp. Bot.* **22**: 756–758.
- Galletti, S., Barillari, J., Iori, R., and Venturi, G. (2006). Glucobrassicin enhancement in woad (*Isatis tinctoria*) leaves by chemical and physical treatments. *J. Sci. Food Agric.* **86**: 1833–1838.
- Glauser, G., Schweizer, F., Turlings, T.C., and Reymond, P. (2012). Rapid profiling of intact glucosinolates in *Arabidopsis* leaves by UHPLC-QTOFMS using a charged surface hybrid column. *Phytochem. Anal.* **23**: 520–528.
- Glock, C., Heumüller, M., and Schuman, E.M. (2017). mRNA transport and local translation in neurons. *Curr. Opin. Neurobiol.* **45**: 169–177.
- Guan, P., Schmidt, F., Riemann, M., Fischer, J., Thines, E., and Nick, P. (2020). Hunting modulators of plant defence: The grapevine trunk disease fungus *Eutypa lata* secretes an amplifier for plant basal immunity. *J. Exp. Bot.* **71**: 3710–3724.
- Hamburger, M. (2002). *Isatis tinctoria*—from the rediscovery of an ancient medicinal plant towards a novel anti-inflammatory phytopharmaceutical. *Phytochem. Rev.* **1**: 333–344.
- Heinlein, M., Epel, B.L., Padgett, H.S., and Beachy, R.N. (1995). Interaction of tobamovirus movement proteins with the plant cytoskeleton. *Science* **270**: 1983–1985.
- Himmelspach, R., Wymer, C.L., Lloyd, C.W., and Nick, P. (1999). Gravity-induced reorientation of cortical microtubules observed. *in vivo*. *Plant J.* **18**: 449–453.
- Hohenberger, P., Eing, C., Straessner, R., Durst, S., Frey, W., and Nick, P. (2011). Plant actin controls membrane permeability. *Biochim. Biophys. Acta, Biomembr.* **9**: 2304–2312.
- Jack, D.B. (1997). One hundred years of aspirin. *Lancet* **350**: 437–439.
- Jordan, A., Hadfield, J.A., Lawrence, N.J., and McGown, A.T. (1998). Tubulin as a target for anticancer drugs: Agents which interact with the mitotic spindle. *Med. Res. Rev.* **18**: 259–296.

- Jordan, M.A., Thrower, D., and Wilson, L. (1991). Mechanism of inhibition of cell proliferation by *Vinca alkaloids*. *Cancer Res.* **51**: 2212–2222.
- Karakaş, Ö. (2019). Effects of methyl jasmonate and putrescine on tryptanthrin and indirubin production in *in vitro* cultures of *Isatis demiriziana* Misirdali. *Int. J. Sec. Metabolites* **6**: 241–250.
- Katz, E., Nisani, S., and Chamovitz, D.A. (2018). Indole-3-carbinol: A plant hormone combatting cancer. *Faculty Rev. F1000Research* **7**: 687.
- Kaul, R., Risinger, A.L., and Mooberry, S.L. (2019). Microtubule-targeting drugs: More than antimetotics. *J. Nat. Prod.* **82**: 680–685.
- Kefeli, V., Kutáček, M., and Vacková, K. (1970). Influence of natural substances of phenolic character and diethylthiocarbamate on metabolism of L-tryptophan in cabbage, maize and pea. *Biol. Plant.* **2**: 81–90.
- Kumagai, F., Yoneda, A., Tomida, T., Sano, T., Nagata, T., and Hasezawa, S. (2001). Fate of nascent microtubules organized at the M/G1 interface, as visualized by synchronized tobacco BY-2 cells stably expressing GFP-tubulin: Time-sequence observations of the reorganization of cortical microtubules in living plant cells. *Plant Cell Physiol.* **42**: 723–732.
- Kumar, V.S., and Navaratnam, V. (2013). Neem (*Azadirachta indica*): Prehistory to contemporary medicinal uses to humankind. *Asian Pac. J. Trop. Bio.* **3**: 505–514.
- Laporte, C., Vetter, G., Loudes, A.-M., Robinson, D.G., Hillmer, S., Stussi-Garaud, C., and Ritzenthaler, C. (2003). Involvement of the secretory pathway and the cytoskeleton in intracellular targeting and tubule assembly of grapevine fanleaf virus movement protein in tobacco BY-2 cells. *Plant Cell* **15**: 2058–2075.
- Lauber, M.A., Koza, S.M., McCall, S.A., Alden, B.A., Iraneta, P.C., and Fountain, K.J. (2013). High-resolution peptide mapping separations with MS-friendly mobile phases and charge-surface-modified C18. *Anal. Chem.* **85**: 6936–6944.
- Li, S.Z. (1578). *Bencao Gangmu: Compendium of Materia Medica*, 6 volumes, Beijing, Foreign Languages Press, 2003 (English translation).
- Lin, C.W., Tsai, F.J., Tsai, C.H., Lai, C.C., Wan, L., Ho, T.Y., Hsieh, C.C., and Chao, P.D.L. (2005). Anti-SARS coronavirus 3C-like protease effects of *Isatis indigotica* root and plant-derived phenolic compounds. *Antivir. Res.* **68**: 36–42.
- Liu, S.-L., Zhang, Z.L., Tian, Z.Q., Zhao, H.-S., Liu, H., Sun, E.Z., Xiao, G.F., Zhang, W., Wang, H.Z., and Pang, D.W. (2012). Effectively and efficiently dissecting the infection of influenza virus by quantum-dot-based single-particle tracking. *ACS Nano* **6**: 141–150.
- Liu, S.L., Zhang, L.J., Wang, Z.G., Zhang, Z.L., Wu, Q.M., Sun, E.Z., Shi, Y.B., and Pang, D.W. (2014). Globally visualizing the microtubule-dependent transport behaviors of influenza virus in live cells. *Anal. Chem.* **86**: 3902–3908.
- Lu, W., and Gelfand, V.I. (2017). Moonlighting motors: Kinesin, dynein, and cell polarity. *Trends Cell Biol.* **27**: 505–514.
- Mahaddalkar, T., and Lopus, M. (2017). From natural products to designer drugs: Development and molecular mechanisms action of novel anti-microtubule breast cancer therapeutics. *Curr. Top. Med. Chem.* **17**: 2559–2568.
- Mahdi, J.G. (2010). Medicinal potential of willow: A chemical perspective of aspirin discovery. *J. Saudi Chem. Soc.* **14**: 317–322.
- Mak, N.K., Leung, C.Y., Wei, X.Y., Shen, X.L., Wong, R.N.S., Leung, K. N., and Fung, M.C. (2004). Inhibition of RANTES expression by indirubin in influenza virus-infected human bronchial epithelial cells. *Biochem. Pharmacol.* **67**: 167–174.
- Mi, L., Gan, N., Cheema, A., Dakshanamurthy, S., Wang, X., Yang, D.C., and Chung, F.L. (2009). Cancer preventive isothiocyanates induce selective degradation of cellular α - and β -tubulins by proteasomes. *J. Biol. Chem.* **284**: 17039–17051.
- Michajlovskij, N., Sedlak, J., Jusic, M., and Buzina, R. (1970). Goitrogenic substances of kale and their possible relations to the endemic goitre on the island of Krk (Yugoslavia). *Physiol. Bohemoslovaca.* **3**: 65–72.
- Mohan, L., Raghav, D., Ashraf, S.M., Sebastian, J., and Rathinasamy, K. (2018). Indirubin, a bis-indole alkaloid binds to tubulin and exhibits antimetabolic activity against HeLa cells in synergism with vinblastine. *Biomed. Pharmacother.* **105**: 506–517.
- Mohn, T., Cutting, B., Ernst, B., and Hamburger, M. (2007). Extraction and analysis of intact glucosinolates—A validated pressurized liquid extraction/liquid chromatography–mass spectrometry protocol for *Isatis tinctoria*, and qualitative analysis of other cruciferous plants. *J. Chromatogr. A* **1166**: 142–151.
- Mohn, T., and Hamburger, M. (2008). Glucosinolate pattern in *Isatis tinctoria* and *I. indigotica* seeds. *Planta Med.* **74**: 885–888.
- Mohn, T., Plitzko, I., and Hamburger, M. (2009). A comprehensive metabolite profiling of *Isatis tinctoria* leaf extracts. *Phytochemistry* **70**: 924–934.
- Muroyama, A., and Lechler, T. (2017). Microtubule organization, dynamics and functions in differentiated cells. *Development* **144**: 3012–3021.
- Naghavi, M.H., and Walsh, D. (2017). Microtubule regulation and function during virus infection. *J. Virol.* **91**: e00538–00517.
- Newman, D.J., and Cragg, G.M. (2020). Natural products as sources of new drugs over the nearly four decades from 01/1981 to 09/2019. *J. Nat. Prod.* **83**: 770–803.
- Nguyen, T., Jamali, A., Grand, E., Morreel, K., Marcelo, P., Gontier, E., and Dauwe, R. (2017). Phenylpropanoid profiling reveals a class of hydroxycinnamoyl glucaric acid conjugates in *Isatis tinctoria* leaves. *Phytochemistry* **144**: 127–140.
- Nick, P., Heuing, A., and Ehmann, B. (2000). Plant chaperonins: A role in microtubule-dependent wall-formation? *Protoplasma* **211**: 234–244.
- Nogales, E., Wolf, S.G., Khan, I.A., Ludueña, R.F., and Downing, K.H. (1995). Structure of tubulin at 6.5 Å and location of the taxol-binding site. *Nature* **375**: 424–427.
- Ouko, M.O., Sambade, A., Brandner, K., Niehl, A., Peña, E., Ahad, A., Heinlein, M., and Nick, P. (2010). Tobacco mutants with reduced microtubule dynamics are less susceptible to TMV. *Plant J.* **62**: 829–839.
- Øverby, A., Bævre, M.S., Thangstad, O.P., and Bones, A.M. (2015). Disintegration of microtubules in *Arabidopsis thaliana* and bladder cancer cells by isothiocyanates. *Front. Plant Sci.* **6**: 6.
- Page, J.E., Balza, F., Nishida, T., and Towers, G.N. (1992). Biologically active diterpenes from *Aspilia mossambicensis*, a chimpanzee medicinal plant. *Phytochemistry* **10**: 3437–3439.
- Peterson, J.R., and Mitchison, T.J. (2002). Small molecules, big impact: A history of chemical inhibitors and the cytoskeleton. *Chem. Biol.* **9**: 1275–1285.
- Rai, A., Kapoor, S., Singh, S., Chatterji, B.P., and Panda, D. (2015). Transcription factor NF- κ B associates with microtubules and stimulates apoptosis in response to suppression of microtubule dynamics in MCF-7 cells. *Biochem. Pharmacol.* **93**: 277–289.
- Rajabi, F., Heene, E., Maisch, J., and Nick, P. (2017). Combination of plant metabolic modules yields synthetic synergies. *PLoS One* **12**: 0169778.
- Recio, M.C., Cerdá-Nicolás, M., Hamburger, M., and Ríos, J.L. (2006a). Anti-arthritis activity of a lipophilic woad (*Isatis tinctoria*) extract. *Planta Med.* **72**: 715–720.
- Recio, M.C., Cerdá-Nicolás, M., Potterat, O., Hamburger, M., and Ríos, J.L. (2006b). Anti-inflammatory and antiallergic activity *in vivo* of lipophilic *Isatis tinctoria* extracts and tryptanthrin. *Planta Med.* **72**: 539–546.
- Sano, T., Higaki, T., Oda, Y., Hayashi, T., and Hasezawa, S. (2005). Appearance of actin microfilament 'twin peaks' in mitosis and their function in cell plate formation, as visualized in tobacco BY-2 cells expressing GFP-fimbrin. *Plant J.* **44**: 595–605.

- Schmitz, M.H., Held, M., Janssens, V., Hutchins, J.R., Hudecz, O., Ivanova, E., Goris, J., Trinkle-Mulcahy, L., Lamond, A.I., Poser, I., Hyman, A.A., Mechtler, K., Peters, J.M., and Gerlich, D.W. (2010). Live-cell imaging RNAi screen identifies PP2A-B55 alpha and importin-beta1 as key mitotic exit regulators in human cells. *Nat. Cell Biol.* **12**: 886–893.
- Schwarzerová, K., Zelenková, S., Nick, P., and Opatrný, Z. (2002). Aluminum-induced rapid changes in the microtubular cytoskeleton of tobacco cell lines. *Plant Cell Physiol.* **43**: 207–216.
- Sethi, G., Ahn, K.S., Sandur, S.K., Lin, X., Chaturvedi, M.M., and Agarwal, B.B. (2006). Indirubin enhances tumor necrosis factor-induced apoptosis through modulation of nuclear factor- κ B signaling pathway. *J. Biol. Chem.* **281**: 23425–23435.
- Shen, B. (2015). A new golden age of natural products drug discovery. *Cell* **163**: 1297–1300.
- Simpson, C., and Yamauchi, Y. (2020). Microtubules in influenza virus entry and egress. *Viruses-Basel* **12**: 117.
- St Johnston, D., and Nüsslein-Volhard, C. (1992). The origin of pattern and polarity in the *Drosophila* embryo. *Cell* **68**: 201–219.
- Tsugawa, H., Cajka, T., Kind, T., Ma, Y., Higgins, B., Ikeda, K., Kanazawa, M., VanderGheynst, J., Fiehn, O., and Arita, M. (2015). MS-DIAL: Data-independent MS/MS deconvolution for comprehensive metabolome analysis. *Nat. Methods* **12**: 523–526.
- Ullah, I., Wakeel, A., Shinwari, Z.K., Jan, S.A., Khalil, A.T., and Ali, M. (2017). Antibacterial and antifungal activity of *Isatis tinctoria* L.(brassicaceae) using the micro-plate method. *Pak. J. Bot.* **49**: 1949–1957.
- Verhoeven, D.T., Goldbohm, R.A., van Poppel, G., Verhagen, H., and van den Brandt, P.A. (1996). Epidemiological studies on brassica vegetables and cancer risk. *Cancer Epidemiol. Biomarkers. Prev.* **5**: 733–748.
- Waller, F. (1998). Phytotherapie der traditionellen chinesischen Medizin. *Zeitschrift für Phytotherapie* **19**: 77–91.
- Wang, I.H., Burckhardt, C.J., Yakimovich, A., Morf, M.K., and Greber, U.F. (2017). The nuclear export factor CRM1 controls juxta-nuclear microtubule-dependent virus transport. *J. Cell Sci.* **130**: 2185–2195.
- Wang, Y., Yang, Z., Zhao, S., Qin, S., Guan, W., Zhao, Y., Lin, Q., and Mo, Z. (2011). Screening of anti-H1N1 active constituents from *Radix isatidis*. *J. Guangzhou Univ. Tradit. Chin. Med.* **28**: 419–422.
- Wiesler, B., Wang, Q.Y., and Nick, P. (2002). The stability of cortical microtubules depends on their orientation. *Plant J.* **32**: 1023–1032.
- Xu, H.Y., Zhang, Y.Q., Liu, Z.M., Chen, T., Lv, C.Y., Tang, S.H., Zhang, X.B., Zhang, W., Li, Z.Y., and Zhou, R.R. (2019). ETCM: An encyclopaedia of traditional Chinese medicine. *Nucleic Acids Res.* **47**: 976–982.
- Yang, Y., Islam, M.S., Wang, J., Li, Y., and Chen, X. (2020). Traditional Chinese medicine in the treatment of patients infected with 2019-new coronavirus (SARS-CoV-2): A review and perspective. *Int. J. Biol. Sci.* **16**: 1708–1717.
- Zhang, L.J., Xia, L., Liu, S.L., Sun, E.Z., Wu, Q.M., Wen, L., Zhang, Z.L., and Pang, D.W. (2018). A “driver switchover” mechanism of influenza virus transport from microfilaments to microtubules. *ACS Nano* **12**: 474–484.
- Zhou, W., and Zhang, X.Y. (2013). Research progress of Chinese herbal medicine *Radix isatidis* (Banlangen). *Am. J. Chin. Med.* **41**: 743–764.

SUPPORTING INFORMATION

Additional Supporting Information may be found online in the supportinformationtab for this article: <http://onlinelibrary.wiley.com/doi/10.1111/jipb.13177/supinfo>

Figure S1. Representative high-performance liquid chromatography chromatograms illustrating the fractionation of *Isatis tinctoria* leaves extracted with MeOH/H₂O 8:2 (A) and ethyl acetate (EtOAc) (B), as well

as *I. tinctoria* roots extracted with MeOH/H₂O 8:2 (C) and EtOAc (D) The interesting candidate fractions are highlighted upon corresponding peaks.

Figure S2. Microtubules in the marker line Bright Yellow 2 α -tubulin 3 green fluorescent protein (BY-2 TuA3-GFP) after 1 h treatment with fractions of *Isatis tinctoria* leaves extracted with MeOH/H₂O 8:2

Geometrical projections from z-stacks collected at z-intervals of 0.5 μ m. White arrows indicate sites of microtubule disassembly.

Figure S3. Exemplary time courses of the microtubular response in the marker line Bright Yellow 2 α -tubulin 3 green fluorescent protein (BY-2 TuA3-GFP) for candidate fractions obtained from the MeOH/H₂O 8:2 leaf extract

(A) ML-4; (B) ML-5; and (C) ML-10.

Figure S4. Microtubules in the marker line Bright Yellow 2 α -tubulin 3 green fluorescent protein (BY-2 TuA3-GFP) after 1 h treatment with fractions of *Isatis tinctoria* leaves extracted with ethyl acetate (EtOAc) Geometrical projections from z-stacks collected at z-intervals of 0.5 μ m. White arrows indicate sites of microtubule disassembly.

Figure S5. Exemplary time courses of the microtubular response in the marker line Bright Yellow 2 α -tubulin 3 green fluorescent protein (BY-2 TuA3-GFP) for candidate fractions obtained from the ethyl acetate (EtOAc) leaf extract

(A) EL-3; and (B) EL-9.

Figure S6. Microtubules in the marker line Bright Yellow 2 α -tubulin 3 green fluorescent protein (BY-2 TuA3-GFP) after 1 h treatment with fractions of *Isatis tinctoria* roots extracted with MeOH/H₂O 8:2 Geometrical projections from z-stacks collected at z-intervals of 0.5 μ m. White arrows indicate sites of microtubule disassembly.

Figure S7. Exemplary time courses of the microtubular response in the marker line Bright Yellow 2 α -tubulin 3 green fluorescent protein (BY-2 TuA3-GFP) for candidate fraction MR-1 obtained from the MeOH/H₂O 8:2 root extract

(A) View on a cell file; (B) zoom in of the white square in A to show the mild disintegration.

Figure S8. Microtubules in the marker line Bright Yellow 2 α -tubulin 3 green fluorescent protein (BY-2 TuA3-GFP) after 1 h treatment with fractions of *Isatis tinctoria* roots extracted with ethyl acetate (EtOAc) Geometrical projections from z-stacks collected at z-intervals of 0.5 μ m. White arrows indicate sites of microtubule disassembly.

Figure S9. Exemplary time courses of the microtubular response in the marker line Bright Yellow 2 α -tubulin 3 green fluorescent protein (BY-2 TuA3-GFP) for candidate fraction ER-9 obtained from the ethyl acetate (EtOAc) leaf extract

(A) View on a cell file; (B) zoom in of the white square in A to show the mild disintegration.

Figure S10. Quantification of actin filaments density for methanolic root fraction MR-1 in expanding cells of the actin marker line *Nicotiana tabacum* L. cv Bright Yellow-2 fimbrin actin-binding protein domain green fluorescent protein (BY-2 FABD2-GFP) 30 min after application

The actin filaments density in response to MR-1 in dilutions of 1:5 and 1:10 were analyzed quantitatively by ImageJ, as compared to the solvent control treatment. Error bars indicate SE of the mean. Different lowercase letters show significance at $P = 5\%$.

Figure S11. Quantification of microtubule integrity of different chemicals in the microtubule marker line *Nicotiana tabacum* L. cv line Bright Yellow 2 α -tubulin 3 green fluorescent protein (BY-2 TuA3-GFP)

The microtubule integrity in response to the solvent (1% dimethyl sulfoxide), epigallocatechin gallate (50 μ mol/L), progoitrin (50 μ mol/L), glucobrassicin (50 μ mol/L), and indirubin (50 μ mol/L) after 60 min of treatment were analyzed quantitatively by ImageJ, as compared to the negative control cells. Error bars indicate SE of the mean. Different lowercase letters show significance at $P = 5\%$.

Figure S12. Microtubular responses of *Nicotiana tabacum* L. cv line Bright Yellow 2 α -tubulin 3 green fluorescent protein (BY-2 TuA3-GFP) cells for the solvent (1% dimethyl sulfoxide, A), combination of 50 μ mol/L epigallocatechin gallate and 50 μ mol/L progoitrin (B), 500 μ mol/L epigallocatechin gallate (C), 500 μ mol/L progoitrin (D), 500 μ mol/L indirubin (E) after 60 min of treatment observed by spinning-disc microscopy

Geometrical projections from z-stacks collected intervals of 0.5 μ m are shown. Lower row shows zoom-ins of the region marked by the white box in the upper row.

Figure S13. Quantification of microtubule integrity for glucobrassicin in HeLa cells expressing a green fluorescent protein (GFP)-tubulin marker

The microtubule integrity in response to 50 μ mol/L glucobrassicin in an

Glucobrassicin eliminates plant microtubules

exemplary time course of 30 and 90 min were analyzed quantitatively by ImageJ, as compared to the control treatment at 0 and 60 min. Error bars indicate *SE* of the mean. Different lowercase letters show significance at $P = 5\%$.

Figure S14. Cell mortality of *Nicotiana tabacum* L. cv Bright Yellow-2 after 24 h incubation with epiprogoitrin, progoitrin, glucobrassicin, and indirubin in a concentration of $50 \mu\text{mol/L}$.

The relative frequency of dead cells was scored samples of 1 500 cells. Data represent three independent biological replicates.

Table S1. Yields of *Isatis tinctoria* leaf and root extractions

Table S2. Gradient conditions used for high-performance liquid chromatography fractionation of the crude plant extracts ($\text{H}_2\text{O} + 0.1\% \text{HCOOH}$ (A) and

$\text{CH}_3\text{CN} + 0.1\% \text{HCOOH}$ (B), 1 mL/min, Uptisphere HDO $3 \mu\text{m}$, $4.6 \times 150 \text{mm}$)
The ratio of the mobile phase eluents are expressed in %B

Table S3. High-performance liquid chromatography fractionation the *Isatis tinctoria* crude extracts at fixed intervals of 3.5 min

Table S4. List of main constituents detected in the MR-1 fraction of the MeOH/ H_2O 8:2 extract from *Isatis tinctoria* root using ultra-high-performance liquid chromatography – high-resolution tandem mass spectrography (UHPLC-HRMS/MS)

Compounds were identified with the MS-DIAL software based on t_R information, accurate masses, and MS/MS data.

Table S5. Overview of results obtained after live-cell visualization of microtubules with confocal microscopy



Scan using WeChat with your smartphone to view JIPB online



Scan with iPhone or iPad to view JIPB online